Discrete breathers in a two-dimensional spring-mass lattice

2009 J. Phys. A: Math. Theor. 42 355207

(http://iopscience.iop.org/1751-8121/42/35/355207)

IOP PUBLISHING JOURNAL OF PHYSICS A: MATHEMATICAL AND THEORETICAL

J. Phys. A: Math. Theor. **42** (2009) 355207 (26pp) doi:10.1088/1751-8113/42/35/355207

Discrete breathers in a two-dimensional spring-mass lattice

Xiang Yi, Jonathan A D Wattis, Hadi Susanto and Linda J Cummings

Theoretical Mechanics, School of Mathematical Sciences, University of Nottingham, University Park, Nottingham, NG7 2RD, UK

E-mail: pmxxy@nottingham.ac.uk, jonathan.wattis@nottingham.ac.uk, hadi.susanto@nottingham.ac.uk and linda.j.cummings@njit.edu

Received 16 January 2009, in final form 3 June 2009
Published 12 August 2009
Online at stacks.iop.org/JPhysA/42/355207

Abstract

We consider a two-dimensional spring-mass lattice with square symmetry in which each particle experiences a nonlinear onsite potential and nonlinear nearest-neighbour interactions. At equilibrium, the particles are equally spaced in both the horizontal and vertical directions and all springs are unextended. Motivated by the work of Marin *et al* (1998 *Phys. Lett.* A **248** 225–9, 2001 *Phys. Lett.* A **281** 21–5), we seek a solution in which most of the breather's energy is focused along three chains. We construct an asymptotic approximation to the breather using the method of multiple scales to describe the coherent oscillations in the three main chains that constitute the discrete breather. We reduce the equation of motion to a nonlinear Schrödinger equation for the leading-order term and find a family of solutions, which encompasses both stationary and moving bright soliton solutions. We use numerical simulations of the lattice to verify the shape and velocity of breathers and find that while stationary breathers are found to persist for long times, moving breathers decay by radiating energy in the direction perpendicular to their motion.

PACS numbers: 05.45.−a, 05.45.Yv

(Some figures in this article are in colour only in the electronic version)

1. Introduction

Discrete breathers are time-periodic, spatially localized solutions of nonlinear lattices. Necessary conditions for the existence of discrete breathers in a lattice are the discreteness of the lattice, which gives rise to gaps and cut-offs in the phonon spectrum, paired with its nonlinearity. Furthermore, a breather's frequency (and that of its harmonics) must avoid resonances with the phonon band in order for the breather to be long-lived.

There is a great deal of work on discrete breathers. Early work on higher dimensional systems includes that of Takeno [27, 28], who finds approximations to breather solutions in

one-, two- and three-dimensional lattices by applying Green's function techniques. This led to an approximate analytical expression for the dispersion relation of the breathers. Supplementary work by Campbell and co-authors [8, 9] gives a simplified argument for the existence of breathers and their stability against decay in Klein–Gordon lattices. The rotating-wave approximation has frequently been applied to lattice systems (see, e.g., [8, 9, 29–31]). Using this method, only terms that are resonant with the fundamental frequency of the breather are retained. As error terms and higher harmonics are neglected, it is difficult to quantify the accuracy of the method. The frequency of the discrete breather, denoted by ω_b, is dependent on the amplitude of the breather. Denoting the wavenumber of a phonon by q and its temporal frequency by ω_q, the condition for the breather to be long-lived is that the frequency of the breather (ω_b) must be nonresonant with the phonon spectrum (ω_q), that is, ω_q/ω_b is never a rational number.

There are many results on the existence of discrete breathers in various one-dimensional Hamiltonian lattices of Fermi–Pasta–Ulam–Tsingou (FPUT) and Klein–Gordon (KG) types. Numerical results strongly imply the existence of discrete breathers in such one-dimensional non-integrable Hamiltonian lattices. Flach, Willis and Kladko investigated the origins and features of localized excitations in Klein–Gordon lattices; see [14–17] where it is suggested that the FPUT lattice could indeed support breathers. Moreover, the theory described in [14, 15] holds independently of the lattice dimension, and it is deduced that the existence of nonlinear localized excitation solutions in one-dimensional lattices can be extended to nonlinear localized excitations in higher dimensional lattices.

MacKay and Aubry [20] then established the existence of stationary breathers in a broad range of lattice models, starting with a one-dimensional Hamiltonian lattice with linear coupling between nearest neighbours and a nonlinear onsite potential of the KG type. The proof considers the anti-continuum limit where the model reduces to a discrete array of uncoupled anharmonic oscillators, where analytical breathers can be found exactly. Using the inverse theorem, it is then argued that discrete breathers can exist when a weak coupling is present. Moreover, MacKay and Aubry [20] point out that the breathers are exponentially stable, that is, Nekhoroshev-stable. This form of stability means that if an orbit starts within a distance ϵ of a breather orbit, the trajectory will stay within $\mathcal{O}(\epsilon)$ for at least a time $C\exp(-K/\epsilon B)$ for some positive constants C, K and β. This result has been confirmed by Bambusi [3]. Furthermore, Aubry and Cretegny [2] have shown the existence of a marginal mode which grows linearly in time at any instability threshold, resulting in a necessary condition for having a highly mobile breather.

According to Flach *et al* [13], breather energies have a positive lower bound if the lattice dimension is greater than or equal to a certain critical value d_c. Such d_c depends on the type of nonlinearity present in the system, the dimension of the lattice typically being no more than 2. In dimensions below d_c, as the amplitude of breather tends to zero, the breather's energy approaches zero as its amplitude decreases to zero. At critical dimension d_c, breather energies will approach a positive value E_0 as the amplitude tends to zero. Furthermore, there are no breathers with energies E in the range $0 < E < E_0$ (in other words, there exists a forbidden gap between 0 and E_0). However, for dimensions above d_c, breather energies tend to increase as the amplitude of breather tends to zero.

In this paper, we ultimately consider a system of three coupled one-dimensional lattices. Models of this form have been considered previously, most notably in the biological arena where they are used to model DNA dynamics. These were pioneered in the late 1980s by a variety of authors, for example [10, 18, 24, 32–34], and have been followed up by others more recently [4]. These models typically consider two degrees of freedom per base pair: one radial variable related to the opening of the hydrogen bonds and an angular one related to the twisting

of each base pair relative to the helicoidal structure of the molecule. Analytical approximations for the small amplitude breather are derived by applying the Lagrangian method. And they have numerically checked that the solution of the breather they obtained are stable for long periods of time.

An interesting phenomenon that may be related to breathers can be found in crystals of muscovite mica: the presence of dark lines, which cannot be explained in terms of changed particle tracks. This inspired the investigations of Marin *et al* [21], who conjecture that these lines might be caused by mobile localized breathers of the longitudinal type. By using numerical simulations and experiments on an analogue model, they tested their conjecture. Their results show that mobile longitudinal breathers do exist, and their existence does not require a special shape for the potential or a constrained range of parameters. Moreover, the lattice exhibits a strong directional preference whereby breathers travel for long distances only along lattice directions. Recently, some investigators found that reconstructive transformations in layer silicates can happen at a much lower temperature than the experimental results reported previously. The reason for this phenomenon is given by Archilla *et al* [1], who claim that discrete breathers can play an important role in reconstructive transformations at low temperatures. To verify this, they obtain their parameters for a model of nonlinear vibrations in the cation layer and, through numerical simulations, obtain an expression for the breather's energy. Though there are far fewer breathers than phonons, the energy from breathers is large enough to influence the experimental results.

Butt and Wattis [5, 6] subsequently considered two-dimensional square and hexagonal FPUT lattices with a scalar-valued function at each node and derived small amplitude approximations to discrete breathers in the models. They showed that the lattice equation can be reduced to a cubic nonlinear Schrödinger (NLS) equation in two special cases: the symmetric and asymmetric interaction potential cases. For symmetric interactions, an associated ellipticity constraint was found, i.e. moving breathers only occur for certain wave-vectors. Butt and Wattis [5, 6] also extended the small amplitude expansion to fifth order and derived a higher order NLS equation which more accurately describes the shape and stability properties of the breather envelope in the case of stationary breathers in symmetric potentials.

In this paper, we also consider a two-dimensional monatomic spring-mass lattice with square symmetry. We use interaction potentials that correspond to small amplitude expansions of those used by Marin *et al* in [22, 23]; however, the geometry of our lattice is slightly simpler than the monatomic hexagonal symmetry of [22] and the diatomic square lattice of [23]. In section 2, we apply the semi-discrete multiple-scales method to reduce the governing equations to a nonlinear Schrödinger equation at the leading order. From the result, we find a group of solutions which encompasses both stationary and moving bright soliton solutions. Our analysis shows how the cubic and quartic coefficients in the potential energy function, and the wavenumber of the carrier wave, determine the type of solution. In section 3, we present numerical simulations of such lattices showing that the asymptotically derived modes are indeed long-lived. Finally, we make some general comments on these results and discuss future work.

2. Asymptotic analysis

2.1. Preliminaries

We consider a two-dimensional spring-mass system with square symmetry. The system is constructed from a repeated arrangement of identical particles of unit mass, with the distance between two adjacent particles being h in each direction. Here, we assume that each particle

experiences a nonlinear onsite potential. At equilibrium the particles are spaced regularly in both horizontal and vertical directions, with all the springs unextended. We select an arbitrary site to be site $(0, 0)$ and remaining sites are labelled using the lattice basis vectors $\mathbf{i} = [1, 0]^T$, $\mathbf{j} = [0, 1]^T$. We describe the position of the particle at site $(m, n) = m\mathbf{i} + n\mathbf{j}$ by the vector $(u_{m,n}(t), v_{m,n}(t))$; this expresses the displacement of the particle from its equilibrium position.

We want to derive an expression for the total energy H of the lattice. First, we assume that the onsite potential V_0 of every particle is of the form

$$V_0(r) = \tfrac{1}{2}\Omega^2 r^2 + \tfrac{1}{4}\lambda r^4, \tag{2.1}$$

where Ω and λ are material constants of the spring and $r = \sqrt{u_{m,n}^2 + v_{m,n}^2}$ denotes the magnitude of the displacement of each particle from its equilibrium position. Second, we assume that the elastic potential energy V_s stored by each spring has the form

$$V_s = \tfrac{1}{2}\phi^2 + \tfrac{1}{3}a\phi^3 + \tfrac{1}{4}b\phi^4, \tag{2.2}$$

where ϕ is the extension of the spring. For the horizontal and the vertical springs, the extension is respectively expressed as

$$\phi_{\mathrm{h}} = \sqrt{(h + u_{m+1,n} - u_{m,n})^2 + (v_{m+1,n} - v_{m,n})^2}, \tag{2.3}$$

$$\phi_{\mathrm{v}} = \sqrt{(u_{m+1,n} - u_{m,n})^2 + (h + v_{m+1,n} - v_{m,n})^2}, \tag{2.4}$$

as illustrated in figure 1.

2.2. *Hamiltonian formulation and equations of motion of the FPUT–KG lattices*

The total energy of the system, H, is defined by the sum of the kinetic energies of every particle, the energy due to the springs and the onsite potential energies. Thus,

$$\begin{aligned} H = \sum_m \sum_n \frac{1}{2}\dot{u}_{m,n}^2 + \frac{1}{2}\dot{v}_{m,n}^2 + V_0\Big(\sqrt{u_{m,n}^2 + v_{m,n}^2}\Big) + V_s(\|(u_{m+1,n}, v_{m+1,n}) - (u_{m,n}, v_{m,n})\|) \\ + V_s(\|(u_{m,n+1}, v_{m,n+1}) - (u_{m,n}, v_{m,n})\|), \end{aligned} \tag{2.5}$$

where $\|\cdot\|$ means the distance between the two corresponding particles.

Marin *et al* [21–23] suggest that breathers can be localized, and the moving disturbance is very narrow in the direction perpendicular to the direction of travel. In line with this observation, we seek solutions in which u and v are much smaller than unity apart from in three main chains, i.e. we focus on one main, or central, chain $n = 0$ and two side chains $n = \pm 1$ (see figure 1(*b*)). Thus, we need equations for the six coupled lattices $u_{m,0}$, $u_{m,\pm 1}$, $v_{m,0}$, $v_{m,\pm 1}$.

We now discuss how to obtain the equations of motion for the displacements of these three chains for this spring-mass system. We assume that there is a mode in which the main chain oscillates purely in the horizontal direction, that is, $u_{m,0} \neq 0$, $v_{m,0} = 0$. Then the chains at positions $n = 1$, $n = -1$ should be related by symmetry, with $u_{m,-1} = u_{m,1}$ and $v_{m,-1} = -v_{m,1}$.

First, we derive the main-chain energy H_0, the $n = 0$ term in the sum in (2.5). Later, we will assume that $u_{m,0}$, $u_{m,\pm 1}$ are an order of magnitude larger than $v_{m,\pm 1}$ (see section 2.3 for the specific ansatz used). Applying Hamilton's principle to (2.5) gives equations of motion for the three chains $u_{m,0}$, $u_{m,1}$, $v_{m,1}$:

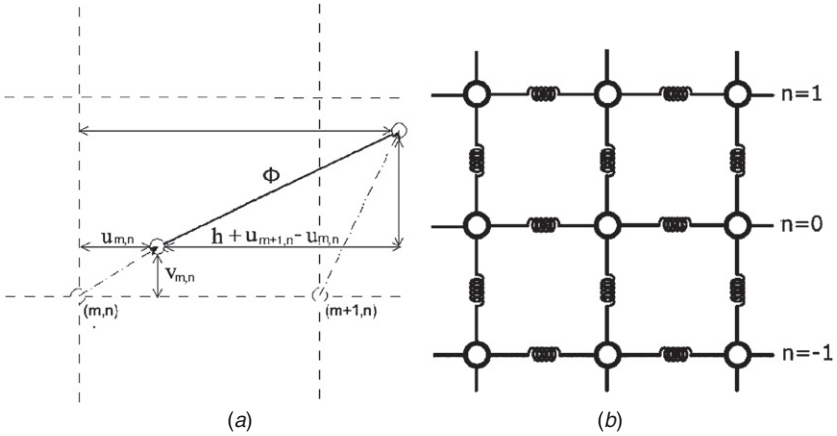

Figure 1. (*a*) The spring connecting particles $P_{m,n}$ and $P_{m+1,n}$ at general time t. (*b*) Illustration of the main chain $n = 0$ (central row) and side chains $n = \pm 1$ (top and bottom rows).

$$\ddot{u}_{m,0} = -\Omega^2 u_{m,0} - \lambda u_{m,0}^3 + (u_{m+1,0} - 2u_{m,0} + u_{m-1,0}) + \frac{2}{h}(u_{m,1} - u_{m,0})v_{m,1}$$
$$+ \frac{1}{h^2}(u_{m,1} - u_{m,0})^3 + a\left[u_{m+1,0}^2 - 2u_{m+1}u_{m,0} + 2u_{m-1,0}u_{m,0} - u_{m-1,0}^2\right]$$
$$+ \frac{2ah-2}{h^2}v_{m,1}^2(u_{m,1}-u_{m,0}) + b[(u_{m+1,0}-u_{m,0})^3 - (u_{m,0}-u_{m-1,0})^3], \tag{2.6}$$

$$\ddot{u}_{m,1} = -\Omega^2 u_{m,1} - \lambda\left(u_{m,1}^2 + v_{m,1}^2\right)u_{m,1} + (u_{m+1,1} - 2u_{m,1} + u_{m-1,1})$$
$$+ \frac{1}{2h}[(v_{m+1,1} - v_{m,1})^2 - (v_{m,1} - v_{m-1,1})^2] + \frac{1}{h}u_{m,0}v_{m,1}$$
$$+ \frac{1}{2h^2}[(u_{m,2} - u_{m,1})^3 - (u_{m,1} - u_{m,0})^3]$$
$$+ a\left[u_{m+1,1}^2 - 2u_{m+1,1}u_{m,1} + 2u_{m-1,1}u_{m,1} - u_{m-1,1}^2\right]$$
$$+ \frac{ah-1}{h^2}[(v_{m+1,1}-v_{m,1})^2(u_{m+1,1}-u_{m,1}) - (v_{m,1}-v_{m-1,1})^2(u_{m,1}-u_{m-1,1})]$$
$$+ b[(u_{m+1,1} - u_{m,1})^3 - (u_{m,1} - u_{m-1,1})^3], \tag{2.7}$$

$$\ddot{v}_{m,1} = -\Omega^2 v_{m,1} - \lambda\left(u_{m,1}^2 + v_{m,1}^2\right)v_{m,1} - 2v_{m,1} + \frac{1}{2h}\left(2u_{m,1}u_{m,0} - u_{m,0}^2\right) + 2bv_{m,1}^3$$
$$+ \frac{1}{h}[(v_{m+1,1} - v_{m,1})(u_{m+1,1} - u_{m,1}) - (v_{m,1} - v_{m-1,1})(u_{m,1} - u_{m-1,1})]$$
$$+ \frac{1}{2h^2}[(v_{m+1,1} - v_{m,1})^3 - (v_{m,1} - v_{m-1,1})^3]$$
$$- \frac{ah-1}{h^2}\left[u_{m,1}^2 v_{m,1} - (u_{m,1} - u_{m,0})^2 v_{m,1}\right] + \frac{ah-1}{h^2}$$
$$\times [(u_{m+1,1} - u_{m,1})^2(v_{m+1,1} - v_{m,1}) - (u_{m,1} - u_{m-1,1})^2(v_{m,1} - v_{m-1,1})]. \tag{2.8}$$

2.3. Asymptotic analysis

We seek small-amplitude breather solutions of (2.6)–(2.8) by applying the semi-discrete multiple-scales method. We introduce new spatial and temporal variables defined by $X = \varepsilon m$, $\tau = \varepsilon t$ and $T = \varepsilon^2 t$, and consider the displacement parameters $u_{m,0}$, $u_{m,1}$ and $v_{m,1}$ to be functions of the independent variables n, t, X, τ and T, of the form

$$u_{m,0}(t) = \varepsilon\,\mathrm{e}^{\mathrm{i}\psi} F + \varepsilon^2 G_0 + \varepsilon^2\,\mathrm{e}^{\mathrm{i}\psi} G_1 + \varepsilon^2\,\mathrm{e}^{2\mathrm{i}\psi} G_2 + \varepsilon^3 H_0 + \varepsilon^3\,\mathrm{e}^{\mathrm{i}\psi} H_1 + \varepsilon^3\,\mathrm{e}^{2\mathrm{i}\psi} H_2 + \varepsilon^3 e^{3i\psi} H_3 + \cdots + \text{c.c.}, \tag{2.9}$$

$$u_{m,1}(t) = \varepsilon\,\mathrm{e}^{\mathrm{i}\psi} P + \varepsilon^2 P_0 + \varepsilon^2\,\mathrm{e}^{\mathrm{i}\psi} P_1 + \varepsilon^2\,\mathrm{e}^{2\mathrm{i}\psi} P_2 + \varepsilon^3 R_0 + \varepsilon^3\,\mathrm{e}^{\mathrm{i}\psi} R_1 + \varepsilon^3\,\mathrm{e}^{2\mathrm{i}\psi} R_2 + \varepsilon^3\,\mathrm{e}^{3\mathrm{i}\psi} R_3 + \cdots + \text{c.c.}, \tag{2.10}$$

$$v_{m,1}(t) = \varepsilon^2 Q_0 + \varepsilon^2\,\mathrm{e}^{\mathrm{i}\psi} Q_1 + \varepsilon^2\,\mathrm{e}^{2\mathrm{i}\psi} Q_2 + \varepsilon^3 S_0 + \varepsilon^3\,\mathrm{e}^{\mathrm{i}\psi} S_1 + \varepsilon^3\,\mathrm{e}^{2\mathrm{i}\psi} S_2 + \varepsilon^3\,\mathrm{e}^{3\mathrm{i}\psi} S_3 + \cdots + \text{c.c.}, \tag{2.11}$$

where $\psi = km + \omega t$, ω and k are the frequency and wavenumber (respectively) of the linear carrier wave, c.c. denotes the complex conjugate and F, G_i, P, etc, are all functions of X, τ and T. Since the imaginary parts of G_0, P_0, Q_0, H_0, R_0 and S_0 do not influence $u_{m,0}$, $u_{m,1}$ and $v_{m,1}$, we will assume that these quantities are real. Substituting ansatzë (2.9)–(2.11) into the equations of motion (2.6)–(2.8) and equating the coefficients of each harmonic in ψ at each order of ε yield equations for the unknown functions in (2.9)–(2.11).

From the $\mathcal{O}(\varepsilon\,\mathrm{e}^{\mathrm{i}\psi})$ terms of $u_{m,0}$ (equation (2.6)), we obtain the dispersion relation

$$\omega = \sqrt{4\sin^2\left(\tfrac{1}{2}k\right) + \Omega^2}. \tag{2.12}$$

From the $\mathcal{O}(\varepsilon^2)$ terms of (2.6), we obtain $0 = -\Omega^2(G_0 + \overline{G}_0)$; thus, $G_0 \equiv 0$.

The order $\mathcal{O}(\varepsilon^2\,\mathrm{e}^{\mathrm{i}\psi})$ terms of equation (2.6) yields

$$2\mathrm{i}\omega F_\tau - \omega^2 G_1 = 2\mathrm{i}\sin k F_X - \left(4\sin^2\left(\tfrac{1}{2}k\right) + \Omega^2\right) G_1; \tag{2.13}$$

after cancelling the G_1 terms due to (2.12), the resulting wave equation is solved by

$$F(X,\tau,T) = F(Z,T), \qquad \text{where} \quad v = -\frac{\sin k}{\omega} = -\frac{\sin k}{\sqrt{4\sin^2\left(\tfrac{1}{2}k\right) + \Omega^2}}. \tag{2.14}$$

The $\mathcal{O}(\varepsilon^2\,\mathrm{e}^{2\mathrm{i}\psi})$ terms of equation (2.6) yield an expression for G_2:

$$G_2 = \frac{16\mathrm{i}a\sin^3\left(\tfrac{1}{2}k\right)\cos\left(\tfrac{1}{2}k\right)F^2}{\Omega^2 + 4\sin^2 k - 4\omega^2}. \tag{2.15}$$

The $\mathcal{O}(\varepsilon^3)$ terms of equation (2.6) give

$$0 = (P - F)\overline{Q}_1 + (\overline{P} - \overline{F})Q_1. \tag{2.16}$$

Next, the $\mathcal{O}(\varepsilon^3\,\mathrm{e}^{\mathrm{i}\psi})$ terms of equation (2.6) give

$$\begin{aligned} 2\mathrm{i}\omega F_T + F_{\tau\tau} + 2\mathrm{i}\omega G_{1\tau} = {} & -3\lambda|F|^2 F + \frac{3}{h^2}(|P|^2 P - P^2\overline{F} + F^2\overline{P} - |F|^2 F) \\ & + \frac{2}{h}[(P - F)(\overline{Q_0} + Q_0) + (\overline{P} - \overline{F})Q_2] - 6b(\cos(2k) - 4\cos k + 3)|F|^2 F \\ & + F_{XX}\cos k + 2\mathrm{i}G_{1X}\sin k + 4a\mathrm{i}\overline{F}G_2\sin k. \end{aligned} \tag{2.17}$$

We anticipate that (2.17) will reduce to a NLS in the variable F on elimination of the other unknown variables, G_2 being given by (2.15). We assume that G_1 represents a perturbation

travelling at the same velocity as F, so that $G_1(X,\tau,T) = G_1(Z,T)$, where $Z = X - v\tau$. Then, by (2.14), the terms involving G_1 disappear from (2.17). It remains to eliminate P, Q_0 and Q_2 from (2.17), which requires consideration of equations (2.7) and (2.8).

From the order $\mathcal{O}(\varepsilon^2\,\mathrm{e}^{\mathrm{i}\psi})$ terms of (2.7), we obtain the dispersion relation (2.12) calculated earlier. The $\mathcal{O}(\varepsilon^2)$ terms of equation (2.7) yield $0 = -\Omega^2(P_0 + \overline{P}_0)$; thus, $P_0 \equiv 0$. The $\mathcal{O}(\varepsilon^2\,\mathrm{e}^{\mathrm{i}\psi})$ terms of equation (2.7) give $P_\tau = -vP_X$, with v as in (2.14). Hence P, like F, is also a travelling wave with velocity v. The $\mathcal{O}(\varepsilon^2\,\mathrm{e}^{2\mathrm{i}\psi})$ terms of equation (2.7) give

$$P_2 = \frac{16\mathrm{i}a\sin^3\left(\frac{1}{2}k\right)\cos\left(\frac{1}{2}k\right)P^2}{\Omega^2 + 4\sin^2 k - 4\omega^2}. \tag{2.18}$$

The $\mathcal{O}(\varepsilon^3)$ terms of equation (2.7) give the relation

$$0 = F\overline{Q}_1 + \overline{F}Q_1, \tag{2.19}$$

that is, $\mathrm{Re}(\overline{F}Q_1) = 0$. Combining (2.19) and (2.16), we see that $P\overline{Q}_1 = -\overline{P}Q_1$. One possibility is clearly $Q_1 = 0$; otherwise $P\overline{Q}_1 = \mathrm{i}\,\alpha$, $F\overline{Q}_1 = \mathrm{i}\,\beta$ for some $\alpha, \beta \in \mathbb{R}$. Then $P = \alpha\,F/\beta$ and $\overline{Q}_1 = \mathrm{i}\,\beta/F$. The latter of these is not possible since it implies $Q_1 \to \infty$, as $X \to \pm\infty$, where $F \to 0$. Hence, we deduce $Q_1 = 0$.

Next, the $\mathcal{O}(\varepsilon^3\mathrm{e}^{\mathrm{i}\psi})$ terms of equation (2.7) give

$$\begin{aligned} 2\mathrm{i}\omega P_T + P_{\tau\tau} + 2\mathrm{i}\omega P_{1\tau} = {} & -3\lambda|P|^2P + \frac{1}{h}[F(\overline{Q_0} + Q_0) + \overline{F}Q_2] \\ & + \frac{3}{2h^2}(P^2\overline{F} - F^2\overline{P} + |F|^2F) + P_{XX}\cos k + 4a\mathrm{i}\overline{P}P_2\sin k. \\ & - 6b(\cos(2k) - 4\cos k + 3)|P|^2P + 2\mathrm{i}P_{1X}\sin k. \end{aligned} \tag{2.20}$$

As with equation (2.17), due to the presence of Q_2 and Q_0 we cannot immediately simplify (2.20). To find how Q_0 and Q_2 are related to P and F, we consider the equation of motion (2.8) for $v_{m,1}$. The $\mathcal{O}(\varepsilon^2)$ terms of equation (2.8) yield

$$Q_0 + \overline{Q_0} = \frac{1}{2h}\frac{F\overline{P} + \overline{F}P - |F|^2}{\Omega^2 + 2}, \tag{2.21}$$

while the $\mathcal{O}(\varepsilon^2\,\mathrm{e}^{\mathrm{i}\psi})$ terms give

$$\omega^2 Q_1 = (\Omega^2 + 2)Q_1, \tag{2.22}$$

so that either $\omega^2 = \Omega^2 + 2$ or $Q_1 \equiv 0$. If the former holds, then from the previous result (2.12), we obtain $\sin^2\left(\frac{1}{2}k\right) = \frac{1}{2}$ which implies that $k = \pm\frac{\pi}{4}, \pm\frac{3\pi}{4}$. This result is unexpected as we obtain only certain discrete wavenumbers instead of a one-parameter family of solutions. Thus, we retain the latter possibility $Q_1 \equiv 0$. Going further to the $\mathcal{O}(\varepsilon^2\,\mathrm{e}^{2\mathrm{i}\psi})$ terms in equation (2.8) gives (using also (2.12))

$$Q_2 = \frac{2FP - F^2}{2h\left(3\Omega^2 + 16\sin^2\left(\frac{1}{2}k\right) - 2\right)}. \tag{2.23}$$

2.4. Coupled NLS equations

We assume $P(X,\tau,T) = P(Z,T)$ and $P_1(X,\tau,T) = P_1(Z,T)$; then we substitute $G_0 = 0$, (2.15), (2.18), $P_0 = 0$, (2.21) and (2.23) into (2.17) and (2.20) to derive the following system of coupled NLS equations, the $\mathcal{O}(\varepsilon^3\mathrm{e}^{\mathrm{i}\psi})$ terms in terms of F equation give

$$2\mathrm{i}\omega F_T = \left(\frac{\sin^2 k}{\Omega^2 + 4\sin^2\left(\frac{1}{2}k\right)} - \cos k\right)F_{ZZ} - 3\lambda|F|^2F + \frac{3}{h^2}(|P|^2P - P^2\overline{F} + F^2\overline{P} - |F|^2F)$$

$$+\frac{1}{h}\left(\frac{F|P|^2+\overline{F}P^2-2|F|^2P-F^2\overline{P}+|F|^2F}{\Omega^2+2}\right.$$
$$\left.+\frac{2F|P|^2-\overline{P}F^2-2|F|^2P+|F|^2F}{3\Omega^2+16\sin^2\left(\frac{1}{2}k\right)-2}\right)$$
$$-6b(\cos(2k)-4\cos k+3)|F|^2F-\frac{64a^2\sin k\sin^3\left(\frac{1}{2}k\right)\cos\left(\frac{1}{2}k\right)}{\Omega^2+4\sin^2 k-4\omega^2}|F|^2F \tag{2.24}$$

and the $\mathcal{O}(\varepsilon^3 e^{i\psi})$ terms in terms of P equation give

$$2i\omega P_T=\left(\frac{\sin^2 k}{\Omega^2+4\sin^2\left(\frac{1}{2}k\right)}-\cos k\right)P_{ZZ}-3\lambda|P|^2P+\frac{3}{2h^2}(P^2\overline{F}-F^2\overline{P}+|F|^2F)$$
$$+\frac{1}{2h^2}\left(\frac{F^2\overline{P}+|F|^2P-|F|^2F}{\Omega^2+2}+\frac{2|F|^2P-|F|^2F}{3\Omega^2+4\sin^2 k-4\omega^2}\right)$$
$$-6b(\cos(2k)-4\cos k+3)|P|^2P-\frac{64a^2\sin k\sin^3\left(\frac{1}{2}k\right)\cos\left(\frac{1}{2}k\right)}{\Omega^2+4\sin^2 k-4\omega^2}|P|^2P. \tag{2.25}$$

Finding explicit solutions to equations (2.24) and (2.25) is considerably more difficult than solving the more commonly studied coupled system

$$iu_t+u_{xx}+(|u|^2+\alpha|v|^2)u=0,\qquad iv_t+v_{xx}+(\alpha|u|^2+|v|^2)v=0. \tag{2.26}$$

In order to simplify the problem (2.24) and (2.25), we make the ansatz $P=\gamma F$, and hence we obtain, from (2.21) and (2.23),

$$Q_0=\frac{(2\gamma-1)|F|^2}{h(\Omega^2+2)},\qquad Q_2=\frac{(1-2\gamma)F^2}{2h\left(3\Omega^2+16\sin^2\left(\frac{1}{2}k\right)-2\right)}. \tag{2.27}$$

Substituting expressions (2.27) into (2.17) then finally yields the NLS equation for F:

$$iF_T+DF_{ZZ}+E|F|^2F=0, \tag{2.28}$$

with

$$D=\left(\frac{\sin^2 k}{\Omega^2+4\sin^2\left(\frac{1}{2}k\right)}-\cos k\right)\Bigg/\left(2\sqrt{\Omega^2+4\sin^2\left(\frac{1}{2}k\right)}\right), \tag{2.29}$$

$$E=-\left[\frac{3}{h^2}(\gamma^3-\gamma^2+\gamma-1)-3\lambda+\frac{2(2\gamma^2-3\gamma+1)}{h^2}\left(\frac{1}{\Omega^2+2}-\frac{1}{6\Omega^2+32\sin^2\left(\frac{1}{2}k\right)-4}\right)\right.$$
$$\left.-\frac{8a(2-\cos k)\sin^2 k}{3\Omega^2+12\sin^2\left(\frac{1}{2}k\right)}-6b(\cos(2k)-4\cos k+3)\right]\Bigg/\left(2\sqrt{\Omega^2+4\sin^2\left(\frac{1}{2}k\right)}\right). \tag{2.30}$$

Provided $DE>0$, (2.28) admits a family of bright soliton solutions of the form

$$F=A\,\mathrm{sech}\left(AZ\sqrt{\frac{E}{2D}}\right)\exp\left(\frac{iEA^2T}{2}\right), \tag{2.31}$$

where the amplitude A is a free parameter. The corresponding solution for $u_{m,0}$, to second order in ε, is

$$u_{m,0}=2\varepsilon A\,\mathrm{sech}\left[\varepsilon A\sqrt{\frac{E}{2D}}\left(m+\frac{t\sin k}{\sqrt{4\sin^2\left(\frac{1}{2}k\right)+\Omega^2}}\right)\right]\cos(J_Ft+km)$$

$$+2a\varepsilon^2A^2\csc^2\left(\frac{1}{2}k\right)\operatorname{sech}^2\left[\varepsilon A\sqrt{\frac{E}{2D}}\left(m+\frac{t\sin k}{\sqrt{4\sin^2\left(\frac{1}{2}k\right)+\Omega^2}}\right)\right]$$
$$\times\left(\cos^2\left(\frac{1}{2}k\right)\cos(2J_Ft+2km)-1\right)+\mathcal{O}(\varepsilon^3), \tag{2.32}$$

where $J_F=\sqrt{4\sin^2(k/2)+\Omega^2}+EA^2\varepsilon^2/2$. The displacements $v_{m,1}$ can also then be found as

$$v_{m,1}=\frac{(1-2\gamma)}{h}\varepsilon^2A^2\operatorname{sech}^2\left[\varepsilon A\sqrt{\frac{E}{2D}}\left(m+\frac{t\sin k}{\sqrt{4\sin^2\left(\frac{1}{2}k\right)+\Omega^2}}\right)\right]$$
$$\times\left[\frac{-1}{\Omega^2+2}+\frac{\cos(2J_Ft+2km)}{\left(6\Omega^2+32\sin^2\left(\frac{1}{2}k\right)-4\right)}\right]. \tag{2.33}$$

2.5. *Equation for proportionality constant* γ

For the displacements $u_{m,1}$, we need the solution P of (2.25). We assume that P is also a bright soliton solution of NLS (2.25) with the same velocity as F, of the form $P(X,\tau,T)=P(Z,T)$. We also write $P_1(X,\tau,T)=P_1(Z,T)$ since P_1 represents a travelling-wave perturbation with the same velocity as F, where, as before, $Z=X-v\tau$ and v is given by (2.14). As with G_1 in equation (2.17), this ansatz causes P_1 to cancel in equation (2.20). Using (2.18) and $F=P/\gamma$, we obtain the NLS equation

$$\mathrm{i}P_T+DP_{ZZ}+M|P|^2P=0, \tag{2.34}$$

with

$$M=-\left[-3\lambda+\frac{3}{2h^2}\left(\frac{1}{\gamma^2}-\frac{1}{\gamma}+1\right)-6b(\cos(2k)-4\cos k+3)\right.$$
$$+\frac{1}{h^2}\left(\frac{1}{\gamma^3}-\frac{2}{\gamma^2}\right)\left(-\frac{1}{\Omega^2+2}+\frac{1}{6\Omega^2+32\sin^2\left(\frac{1}{2}k\right)-4}\right)$$
$$\left.-\frac{8a(2-\cos k)\sin k}{3\Omega^2+12\sin^2\left(\frac{1}{2}k\right)}\right]\Bigg/\left(2\sqrt{\Omega^2+4\sin^2\left(\frac{1}{2}k\right)}\right). \tag{2.35}$$

Because of the relation between F and P, i.e. $P=\gamma F$, we require for consistency

$$E=\gamma^2M,\qquad \gamma\in\mathbb{R}, \tag{2.36}$$

where E appears in the NLS (2.28) for F and is defined by (2.33) and M appears in the NLS (2.34) for P and is defined by (2.35). This can be rewritten as

$$0=3\lambda+\frac{3}{2h^2}\left(\frac{3-3\gamma+3\gamma^2-2\gamma^3}{1-\gamma^2}\right)+48b\sin^4\left(\frac{1}{2}k\right)+\frac{8a(2-\cos k)\sin^2k}{3\Omega^2+12\sin^2\left(\frac{1}{2}k\right)}$$
$$-\frac{(4\gamma^3-6\gamma^2+1)}{h^2\gamma(1-\gamma^2)}\left(\frac{1}{\Omega^2+2}-\frac{1}{6\Omega^2+32\sin^2\left(\frac{1}{2}k\right)-4}\right). \tag{2.37}$$

Equation (2.37) is effectively a quartic polynomial in γ, so we cannot easily obtain an explicit expression for γ. To simplify the problem slightly, we choose $a=0$ and keep $b\neq0$ in expression (2.2) for the nonlinear nearest-neighbour interactions.

In order to find solutions in which the greatest displacements from equilibrium occur on the row $n = 0$, we aim to find solutions with $|\gamma| < 1$ small. To investigate the possibility that γ is very small, we eliminate the $\gamma^2, \gamma^3, \gamma^4$ terms from (2.37), yielding the approximation

$$\left[3\lambda + 48b\sin^4\left(\frac{1}{2}k\right) + \frac{9}{2h^2}\right]\gamma = \frac{1}{(\Omega^2+2)h^2} - \frac{1}{\left(6\Omega^2 + 32\sin^2\left(\frac{1}{2}k\right) - 4\right)h^2}. \tag{2.38}$$

Small values of γ can be caused by any of Ω, λ, h or b being large.

When γ is positive ($0 < \gamma < 1$), we describe the breather oscillations as 'in-phase'. This means that particles in the side chains move in the same direction as those in the main chain. If they move in the opposite direction, we refer the oscillation as 'out-of-phase'; this occurs when γ is negative ($-1 < \gamma < 0$).

2.6. *Stationary breathers in the limit* $\Omega \gg 1$

In order to consider cases where γ is small, we use (2.38) and take $\Omega \gg 1$ with B, h, λ all being $\mathcal{O}(1)$ (and in particular $\varepsilon \ll \gamma \ll 1$).

We know that the NLS equation (2.28) for F admits bright soliton solutions if the coefficients D and E are of the same sign and dark soliton solutions if D and E are of opposite sign [26]. In our case, due to the complexity of the expressions for D and E, it is difficult in general to define the region in k-space where $DE > 0$. It is more sensible to analyse a variety of cases, and we start with the case of stationary breathers, for which the wavenumber is $k = \pi$.

For $k = \pi$, equation (2.29) gives $D_\pi = 1/(2\sqrt{\Omega^2+4})$ which is always positive. We need to clarify which combinations of parameters (Ω, a, b, λ, h, k and γ) make D and E have the same sign, and hence give rise to a bright breather solution. In our analysis, we assume γ to be real. For $k = \pi$, because γ is assumed to be small and we consider Ω to be large ($\Omega \gg 1$), the leading order expression for E using (2.30) is

$$E_\pi \sim \frac{3}{2\Omega}\left(\lambda + \frac{1}{h^2} + 16b\right). \tag{2.39}$$

Thus, for $E_\pi > 0$, we require

$$b > -\frac{1}{16}\left(\frac{1}{h^2} + \lambda\right), \tag{2.40}$$

and stationary bright breather solutions (with $k = \pi$) only exist when (2.40) holds.

2.7. *Moving breathers in the limit* $\Omega \gg 1$

Next, we seek a moving bright breather solution, with $k < \pi$. Rearranging expressions (2.29) and (2.30) for D and E gives, at leading order,

$$D_k \sim -\frac{\cos k}{2\Omega}, \qquad E_k \sim \frac{3}{2\Omega}\left(\lambda + \frac{1}{h^2} + 16b\sin^4\left(\frac{1}{2}k\right)\right). \tag{2.41}$$

Clearly, D_k is small for all k and changes sign near $k = \pi/2$, it being positive for $\pi/2 < k < \pi$. In this region of k, a positive E_k requires

$$b > -\frac{1}{16\sin^4\left(\frac{1}{2}k\right)}\left(\lambda + \frac{1}{h^2}\right). \tag{2.42}$$

For $b > 0$, $\lambda > -1/h^2$, we have $E_k > 0$ for all k and bright breathers exist for the range $\pi > k > k_c \sim \frac{1}{2}\pi$. However, if $\lambda < -1/h^2$ then $E_0 < 0$ and we have $E_k > 0$ for $\pi > k > k_0$

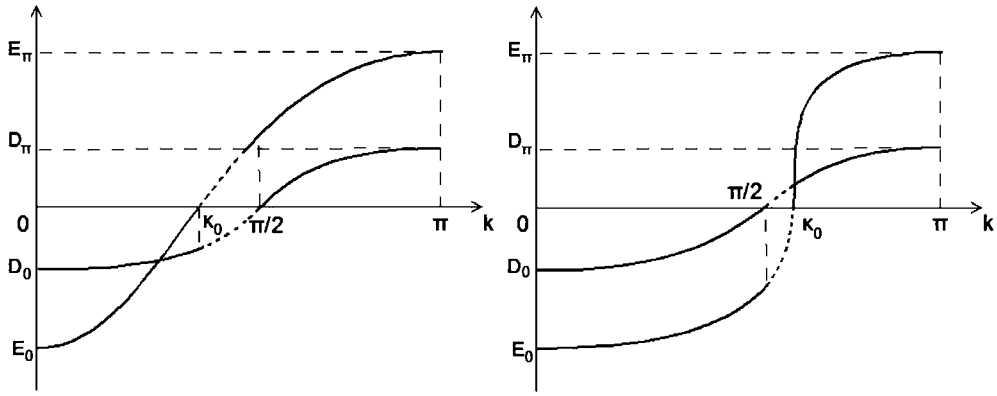

Figure 2. The left plot illustrates how the coefficients D and E change with the wavenumber k when $0 < k_0 < \pi/2$. The dashed line represents those regions in which D and E have opposing signs. This happens when $k_0 < k < \pi/2$ and in these regions, it is not possible to find a bright soliton solution. The right plot covers the case $\pi/2 < k_0 < \pi$. Here, there is no bright soliton solution when $\pi/2 < k < k_0$.

and $E_k < 0$ for $0 < k < k_0$ (for some k_0). In this case, there are two ranges of k in which bright breathers exist. If, in addition to (2.42), $k_0 < \pi/2$, then the ranges are $0 < k < k_0$ and $\pi/2 < k < \pi$.

If $k_0 > \pi/2$, then the ranges are $0 < k < \pi/2$ and $k_0 < k < \pi$. These two scenarios are illustrated in figure 2. The curves for D_k and E_k are solid for those wavenumbers where $D_k E_k > 0$ (where bright breathers exist) and dashed where $D_k E_k < 0$. From (2.41), the critical wavenumber k_0 is given by

$$k_0 \sim 2\sin^{-1}\left(\frac{-1}{16b}\left(\lambda + \frac{1}{h^2}\right)\right)^{1/4}. \tag{2.43}$$

The other cases that we should note are as follows: (i) where $E_k < 0$ for all k (which occurs, for example, when $b < 0$ and $\lambda < -1/h^2$), leading to the existence of bright breathers only for $k < \pi/2$ and not for $\pi/2 < k < \pi$, and (ii) where $E_0 > 0$ and $E_\pi < 0$ (for example, when $b < -(\lambda + 1/h^2)/16$ and $\lambda > -1/h^2$), in which case there is a range of k values between k_0 and $\pi/2$ for which there are moving bright breathers, but none for k in the intervals $(0, \min(k_0, \pi/2))$ or $(\max(k_0, \pi/2), \pi)$.

2.8. Asymptotic estimate for breather energy

In this section we use our solution for $u_{m,0}$, $u_{m,1}$ and $v_{m,1}$ (as given by (2.32), $u_{m,1} \sim \gamma u_{m,0}$ and (2.33)) to find a leading-order estimate for the main-chain energy H_0 and the side-chain energy H_1, as defined by (A.1) and (A.2) respectively.

Defining $\theta = J_F t + km$, we sum the kinetic and potential energies (both onsite and nearest-neighbour terms) to find the leading-order total energy of the central chain:

$$\begin{aligned} H_0 \sim \frac{(2A)^2}{2}\varepsilon^2 \sum_m \operatorname{sech}^2\left[\varepsilon A\sqrt{\frac{E}{2D}}\left(m + \frac{t\sin k}{\sqrt{4\sin^2\left(\frac{1}{2}k\right) + \Omega^2}}\right)\right] \\ \times\left[J_F^2\sin^2\theta + (\cos k - 1)^2\cos^2\theta + \sin^2 k\sin^2\theta\right. \\ \left. - \sin k(\cos k - 1)\sin\theta\cos\theta + \Omega^2\cos^2\theta\right] + \mathcal{O}(\varepsilon^3). \end{aligned} \tag{2.44}$$

We define $\alpha = 2A$ and $\beta = A\sqrt{\frac{E}{2D}}$, and use the results

$$\begin{aligned} \frac{1}{m}\sum_{m}\cos^2(km) &= \langle\cos^2(km)\rangle = \frac{1}{2}, \\ \frac{1}{m}\sum_{m}\sin^2(km) &= \langle\sin^2(km)\rangle = \frac{1}{2}, \end{aligned} \tag{2.45}$$

$$\sum_{m=-\infty}^{\infty}\sin(2\theta)\operatorname{sech}^2\left[\varepsilon\beta\left(m + \frac{t\sin k}{\sqrt{4\sin^2\left(\frac{k}{2}\right)+\Omega^2}}\right)\right] = 0, \tag{2.46}$$

which follow from averaging and symmetry arguments, to transform (2.44) into

$$H_0 \sim 2\varepsilon A\sqrt{\frac{2D}{E}}\left(\Omega^2 + J_F^2 + 4\sin^2\left(\frac{1}{2}k\right)\right). \tag{2.47}$$

Since $P = \gamma\, F$ and $u_{m,1} \sim \gamma\, u_{m,0}$, the expression for the energy in the side chain (A.2) implies

$$\begin{aligned} H_1 \sim \frac{(2A)^2}{2}\gamma^2\varepsilon^2\sum_{m}\operatorname{sech}^2\left[\varepsilon A\sqrt{\frac{E}{2D}}\left(m + \frac{t\sin k}{\sqrt{4\sin^2\left(\frac{k}{2}\right)+\Omega^2}}\right)\right] \\ \times\left[J_F^2\sin^2\theta + (\cos k - 1)^2\cos^2\theta + \sin^2 k\sin^2\theta\right. \\ \left. - \sin k(\cos k - 1)\sin\theta\cos\theta + \Omega^2\cos^2\theta\right] + \mathcal{O}(\varepsilon^3), \end{aligned} \tag{2.48}$$

which can be simplified to

$$H_1 \sim 2\varepsilon A\gamma^2\sqrt{\frac{2D}{E}}\left(\Omega^2 + J_F^2 + 2 - 2\cos k\right). \tag{2.49}$$

In the following section, these asymptotic estimates will be compared to the results of numerical simulations of stationary and moving breathers.

3. Results of numerical simulations

3.1. Initial conditions, boundary conditions and cell energy

In this section we present the results of solving the two-dimensional spring-mass system numerically (using matlab) on a lattice of size $M_S \times N_S$, with $M_S > 100$ and $N_S \geqslant 10$. We aim to verify that the shape and velocity of the stationary and moving waveforms in the main chain and two side chains predicted by our asymptotic method are long-lived in numerical simulations of the system.

For initial conditions we use the asymptotic expressions generated in the previous section, putting $(u_{m,0}, v_{m,0})$ on the line $n = N_S/2$ and $(u_{m,\pm1}, v_{m,\pm1})$ on the lines $n = N_S/2 \pm 1$. By introducing the variables $R_{m,n} = \mathrm{d}u_{m,n}/\mathrm{d}t$ and $S_{m,n} = \mathrm{d}v_{m,n}/\mathrm{d}t$, we convert the systems of second-order ordinary differential equations for $\ddot{u}_{m,n}$ and $\ddot{v}_{m,n}$ into an equivalent first-order system. We apply the periodic boundary conditions

$$\begin{aligned} u_{m,N_S+1}(t) &= u_{m,1}(t), \qquad & u_{m,0}(t) &= u_{m,N_S}(t), \\ u_{M_S+1,n}(t) &= u_{1,n}(t), \qquad & u_{0,n}(t) &= u_{M_S,n}(t), \end{aligned} \tag{3.1}$$

and similarly for $v_{m,n}$ to the discretized system.

We define the energy in one cell of lattice, $e_{m,n}$, by taking the summand of the Hamiltonian (2.5) (see the appendix for full details). Moments of the cell energy, h_q, and the position of the breather, $(m, n) = (X(t), 0)$, are then given by

$$X(t) = \frac{h_1}{h_0}, \qquad \text{where} \quad h_q = \sum_m m^q (e_{m,0} + 2e_{m,1}) \tag{3.2}$$

(the factor of 2 in h_q accounts for the two side chains having equal energy).

To describe the shape of the breather, we introduce its width in the m-direction, defined by $W_{mbr}^2 = \sum_m (m - X(t))^2 (e_{m,0} + 2e_{m,1})/h_0$ or

$$W_{mbr}^2 = \frac{h_2}{h_0} - \frac{h_1^2}{h_0^2}, \tag{3.3}$$

and its width in the n direction, defined as $W_{nbr}^2 = \sum_{m,n} n^2 e_{m,n}/\tilde{h}_0$ or

$$W_{nbr}^2 = \frac{\tilde{h}_2}{\tilde{h}_0} - \frac{\tilde{h}_1^2}{\tilde{h}_0^2}, \qquad \text{where} \quad \tilde{h}_q = \sum_{m,n} n^q e_{m,n}, \qquad q = 0, 1, 2. \tag{3.4}$$

These definitions are motivated by the statistical variance, where the relative energy density $e_{m,n} \big/ \sum_{j,k} e_{j,k}$ is treated as a probability density function.

We use W_{mbr} and W_{nbr} to quantify the distortion suffered by the breather if the profile changes over time. Furthermore, to determine whether the breather loses energy or simply modifies its shape from the approximation used as initial conditions, we also measure the energy localized near the breather, E_{br}:

$$E_{\text{br}} = \sum_{m=X(t)-\delta_m}^{X(t)+\delta_m} \sum_{n=N_S/2-\delta_n}^{N_S/2+\delta_n} e_{m,n}. \tag{3.5}$$

We pick values δ_m and δ_n depending on the lattice sizes (typically $\delta_m = M/4$ and $\delta_n = N_S/4$).

3.2. Stationary breather with $\Omega \gg \mathcal{O}(1)$

First we focus on stationary breather solutions ($k = \pi$) for the parameters $h = 0.3$, $\varepsilon = 0.03$, $A = 1.0$, $a = 0.0$, $b = -0.64$, $\lambda = 0.8$ and $\Omega = 3.0$, in a lattice of size $M_S = 130$, $N_S = 10$ ($1 \leqslant m \leqslant M_S$, $1 \leqslant n \leqslant N_S$). Since solution (2.9)–(2.11), or equivalently (2.32) and (2.33), is invariant under translations of a discrete number of lattice sites, we move the breather so that it is centred at $m = M_S/2$, $n = N_S/2$. In this case, the temporal frequency of the carrier wave is $\omega = 3.6056$, from which it follows that the period of oscillation is $T = 2\pi/\omega = 1.7426$ and, by solving (2.37), $\gamma = 0.04$. For these parameter values, we illustrate the breather displacements in the whole lattice in figure 3.

Figure 3 shows the breather initially situated in the centre of the lattice. After the breather has completed 57 oscillations, it remains highly localized without significant spreading in any direction. In 66 oscillations, the numerically computed value of the main-chain energy (given by (A.1)) reduces from $H_{0,t=0} = 1.4945$ to $H_{0,t=115} = 1.4321$—a small change of $\Delta H_0/H_0 = -4\%$. The computed value $H_0 = 1.4945$ is a good match to our asymptotic estimate of 1.4951 given by (2.47); similar agreement holds for the side chains also, with the computed value (given by (A.2)) and asymptotic estimate (given by (2.49)) of H_1 being 0.0240 and 0.0243 respectively. After 66 oscillations, H_1 rises to 0.0262—an increase of $\Delta H_1/H_1 = 10\%$.

To determine whether a breather continuously loses energy or suffers an initial transient change in shape without losing energy, we focus on the energy in the central part of the lattice, E_{br} (given by (3.5) with the sum taken over $100 \leqslant m \leqslant 300$ and $3 \leqslant n \leqslant 7$) and investigate

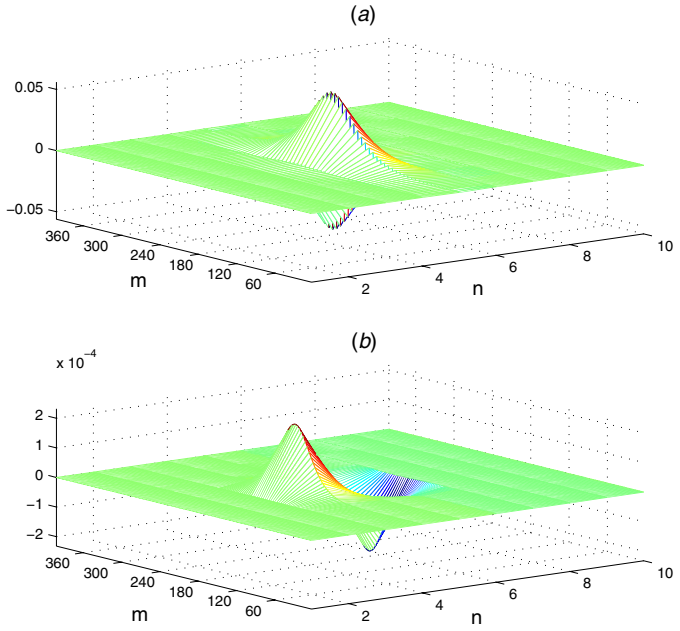

Figure 3. Illustration of a stationary breather in the square lattice for large Ω. The lattice node displacements parallel (u) and perpendicular (v) to the direction of motion of the main chain are shown. (a) u at $t = 0$ and (b) v at $t = 0$. See section 3.2 for further details.

the widths of breather in the m- and n-directions as defined by (3.3) and (3.4), respectively. The energy plot shown in figure 4(a) shows an extremely small variation (around 10^{-9}) as the system is integrated from $t = 0$ to $t = 700$. This is of magnitude similar to the accuracy of the numerical scheme used. The total energy of the system does not fluctuate significantly, that is, $\Delta H/H = 8.8501 \times 10^{-7}$.

However, the graphs of breather width against time (figures 4(b) and (c)) show that the breather gets slightly wider in the m-direction and significantly wider in the n-direction as time progresses. At $t = 0$, the breather width in the m-direction is 28.9709 and only 0.0596 in the n-direction; 700 time units later, the corresponding values are $W_{mbr} = 29.1625$ and $W_{nbr,t=700} = 0.7763$. We observe a slow steady widening of the breather in the m-direction and a more significant widening in the n-direction, though it appears that this might be saturating at larger times and approaching a steady state.

3.3. Moving breather with $\Omega \gg \mathcal{O}(1)$ *and* $k = 2.5$

We now present a simulation of a moving breather with lattice size $M_S = 300$, $N_S = 10$. For this, we choose wavenumber $k = 2.5$, with the remaining parameters $h = 0.3$, $\varepsilon = 0.03$, $A = 1.0$, $a = 0.0$, $b = -0.55$, $\lambda = -0.8$ and $\Omega = 2.5$. Here, the breather frequency is $\omega = 3.1388$, and hence the period is $T = 2.0018$ with the corresponding value for γ being 0.045 (by (2.37)). Hence, the velocity prediction (2.14) is $v_{\text{asy}} = -0.1907$.

The profile of the initial breather, which is located at the centre of the lattice, is shown in figures 5(a) and 6(a). At time $t = 0$, the numerically computed value of the main-chain energy (H_0, given by (A.1)) is close to 0.6213, while our asymptotic estimate of H_0 as given by (2.47) is 0.6214; thus, there is only a tiny change in the computed value with

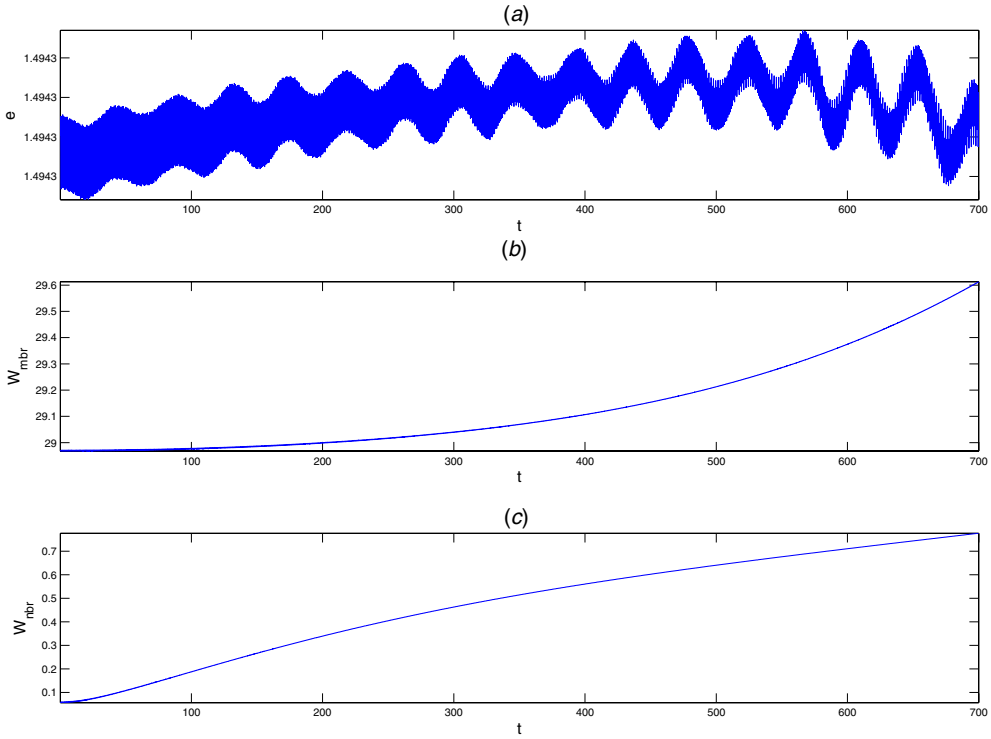

Figure 4. Illustration of how the energy $E_{\rm br}$ (3.5) localized at the breather changes over time, and how the widths W_{mbr} (3.3) and W_{nbr} (3.3) of the breather in the m- and n-directions change from $t = 0$ to $t = 700$ when Ω is large. (a) Central area energy from $t = 0$ to $t = 700$, (b) width in the m-direction from $t = 0$ to $t = 700$ and (c) width in the n-direction from $t = 0$ to $t = 700$. See section 3.2 for more details.

$\Delta H_0/H_{0,t=0} = 1.6095 \times 10^{-4}$. The side chain shows even better agreement where both the computed value and asymptotic estimate give $H_1 = 0.0012$. Figures 5(b) and 6(b) illustrate how the breather has moved along the m-direction at $t = 49.96$, $T = 100$ s. We can see that the general shape of the longitudinal displacement u does not change much compared to the initial time, but the lateral displacement v is elongated in the n-direction, showing some shedding of radiation. Nevertheless, the breather remains well localized in the lattice. Figures 5(c) and 6(c) show the breather at $t = 99.91$, $T = 200$. Both u- and v-components have now spread a little further in the n-direction, albeit at a low level.

The numerically computed value for the central chain energy, $H_0 = 0.5350$, is still of the same order as the initial value. The corresponding value for the side-chain energy is $H_1(t = 200) = 0.0444$, which implies that the central chain of the lattice has lost energy to the side chains as the breather moves. Figures 5(d) and 6(d) show the breather approaching the front edge of the lattice. Although the breather continues to spread slowly as it propagates, it remains well localized after 150 oscillations.

To determine the breather's velocity, we plot position against time (a straight line, not shown) and use its gradient to find the numerical velocity $v_{\rm num} = -0.1899$. The percentage difference from the asymptotic estimate $v = -0.1907$ (given above) is $\Delta v/v_{\rm num} = 0.42\%$—a close match. Figure 7 shows how the width of the breather changes over time in both m-

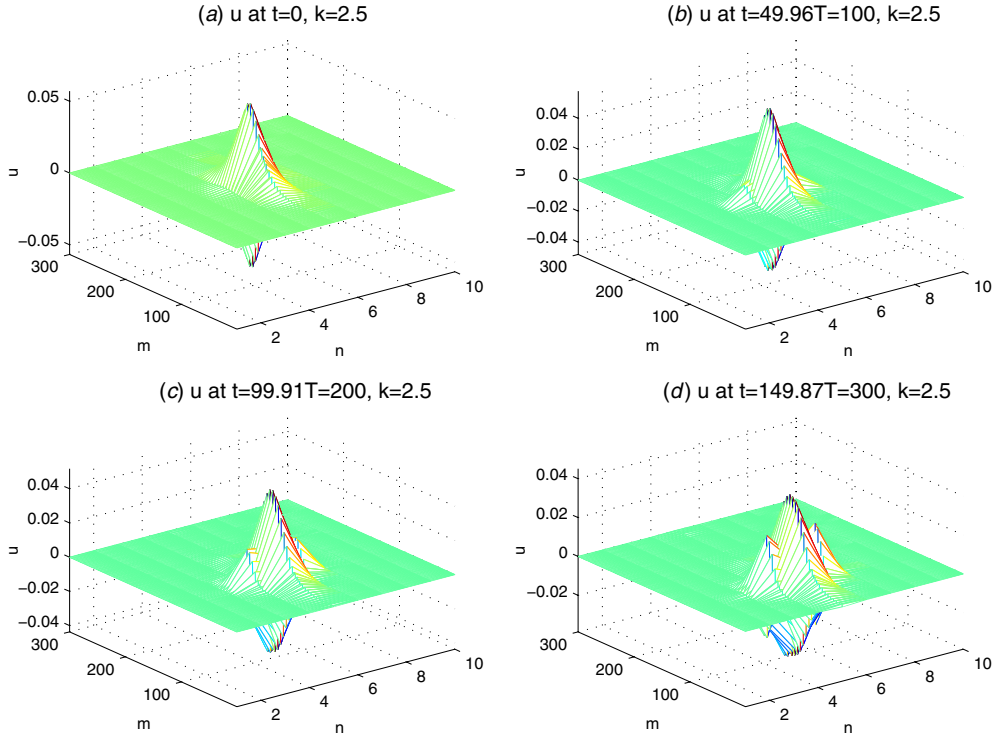

Figure 5. A moving breather in the square lattice, with $k = 2.5$: (*a*) $u_{m,n}$ at $t = 0$; (*b*) $u_{m,n}$ at $t = 49.95T = 100$; (*c*) $u_{m,n}$ at $t = 99.91T = 200$; (*d*) $u_{m,n}$ at $t = 149.87T = 350$. See section 3.3 for more details.

and n-directions. The breather slowly widens in the m-direction from a width of 15.8897 to 16.2033, over 350 time units—a change of 2%. The increase in the width of the breather in the n-direction is more significant: it grows from 0.0647 to 0.5741. However, if we define a box of length 100 in the m-direction and 5 in the n-direction, centred on the breather, and ask how much of the system's energy is within this box, the quantity $E_{\rm br}$, we find a change of only 3×10^{-6} (see (3.5) with $\delta_m = 50$ and $\delta_n = 2$; the value is $E_{\rm br} \approx 0.62$). Such a small difference suggests that it is due to the shape of the breather changing rather than to the breather shedding delocalized radiation to the rest of the lattice. This result supports the proposal that the breather mode is long-lived.

3.4. Moving breather with $\Omega \gg \mathcal{O}(1)$ *and* $k = 0.5$

In the previous section, we presented an example of a moving breather with $k > \pi/2$, that is, to the right of the non-existence gap in figure 2; here we show another simulation of a moving breather, this time with $k < \pi/2$, by choosing $k = 0.5$. We use $h = 1.0$, $\varepsilon = 0.03$, $A = 1.0$, $a = 0$, $b = -1.0$, $\lambda = -1.0$ and $\Omega = 3.0$. The breather frequency is $\omega = 3.0405$, and hence the period of oscillation is $T = 2\pi/\omega = 2.0665$, and solving (2.37) we find $\gamma = 0.0543$. We simulate a lattice of size $M_S = 700$, $N_S = 10$.

Figures 8(*a*) and (*c*) show the breather initially located at the centre of the lattice, with a localized structure. Figures 8(*b*) and (*d*) show the breather at $t = 169.37T = 350$, where it has

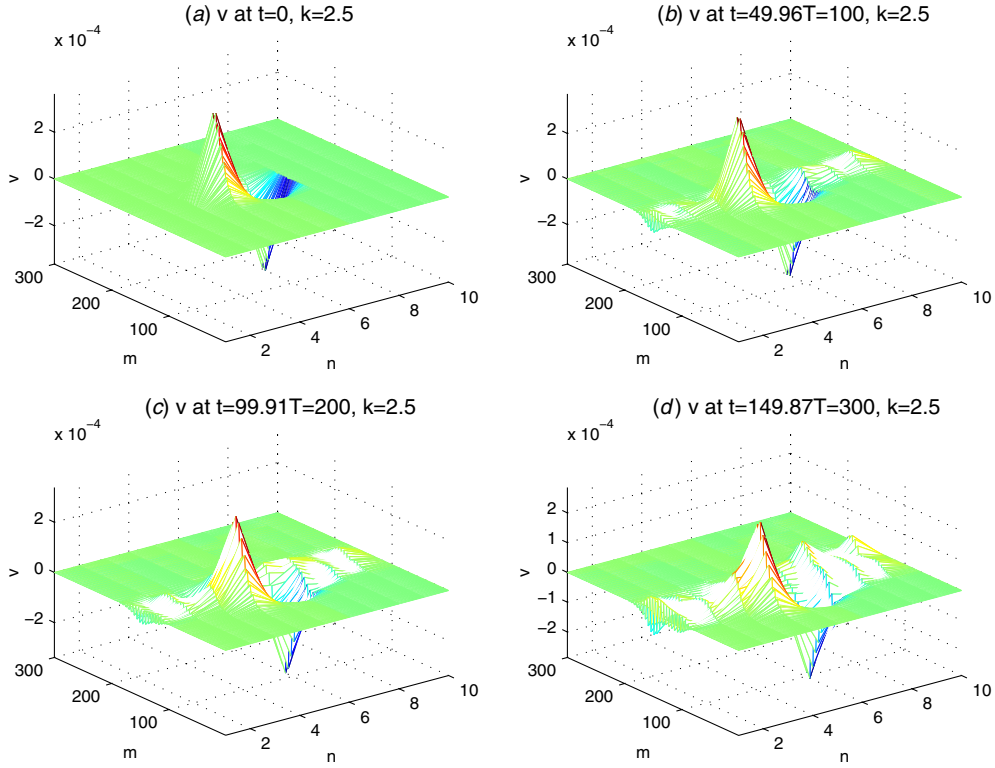

Figure 6. A moving breather in the square lattice, with $k = 2.5$: (*a*) $v_{m,n}$ at $t = 0$; (*b*) $v_{m,n}$ at $t = 49.95T = 100$; (*c*) $v_{m,n}$ at $t = 99.91T = 200$; (*d*) $v_{m,n}$ at $t = 149.87T = 350$. See section 3.3 for more details.

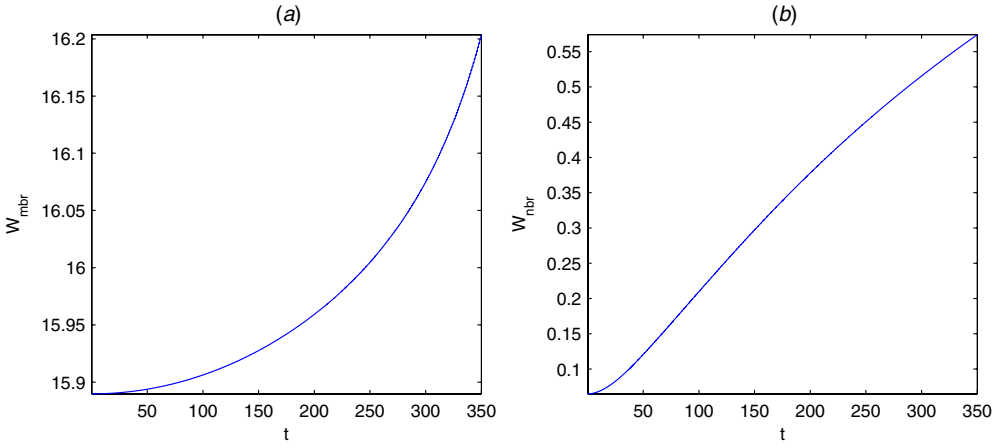

Figure 7. Plot of the breather width against time: (*a*) in the *m*-direction and (*b*) in the *n*-direction, for a moving breather with $k = 2.5$. See section 3.3 for more details.

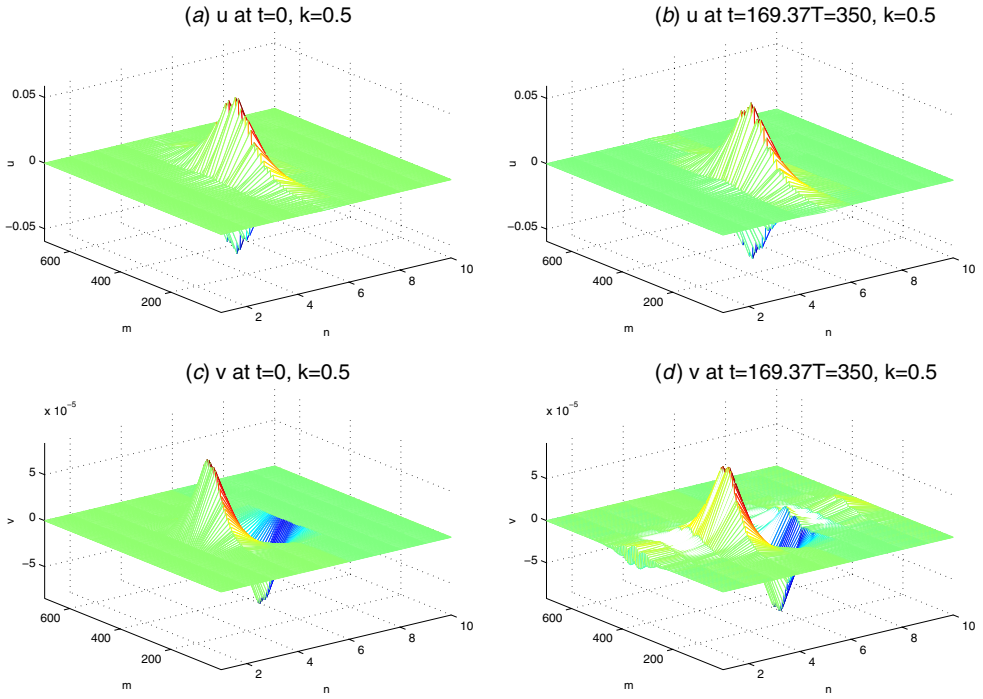

Figure 8. Displacements plotted against position (m, n) in the square lattice at various times, for a moving breather with $k = 0.5$: (a) $u_{m,n}$ at $t = 0$, (b) $u_{m,n}$ at $t = 350$, (c) $v_{m,n}$ at $t = 0$ and (d) $v_{m,n}$ at $t = 350$. See section 3.4 for more details.

travelled forward along the m-direction. The breather has broadened slightly in the n-direction, but remains localized. At $t = 0$, the computed main-chain energy $H_0 = 2.1473$ (from (A.1)) is close to our asymptotic estimate of 2.1474 (obtained using (2.47)). At $t = 350$, the computed central chain energy is $H_0 = 2.1382$, i.e. there is a relatively small decrease. However, the value of the side-chain energy shows a considerable increase, from $H_1(0) = 0.0063$ to $H_1(t = 350) = 0.0109$. This shows a transfer of energy from the central chain to the side chains over time. However, even after 350 time units, $H_1 \ll H_0$ so we observe extreme localization in the n-direction, and it appears that our predicted shape of the breather in the m-direction is accurate.

Figure 9 shows the profile of the main chains at $t = 0$ and at $t = 169.37T = 350$. The breather initially lies at the lattice centre (figures 9(a), (c) and (e)); in figures 9(b), (d) and (f), we see that it has moved significantly to the left, by about 50 lattice sites. This simulation gives a velocity of $v_{\text{num}} = -0.1574$, very close to our asymptotic estimate of $v_{\text{asy}} = -0.1577$ obtained from (2.14), the difference being only $\Delta v/v_{\text{num}} = 0.19\%$. The width in the m-direction increases a little from $W_{mbr} = 58.4695$ at $t = 0$ to 58.5001 at $t = 350$. The width in the n-direction rises from 0.0767 at $t = 0$ to 0.1004 when $t = 350$; this increase is again more significant. Defining a box of width 300 in the m-direction and 5 in the n-direction, centred on the breather's position, we measure the energy E_{br} in the box: the variation between $t = 0$ and $t = 350$ s in E_{br} is 10^{-6}. Such a small difference strongly supports the long-lived nature of the breather mode since it suggests that the variations in the width noted above are initial transient changes of the breather shape, and not an instability by which the breather loses energy to delocalized radiation (which would give a flux of energy to the region outside the box).

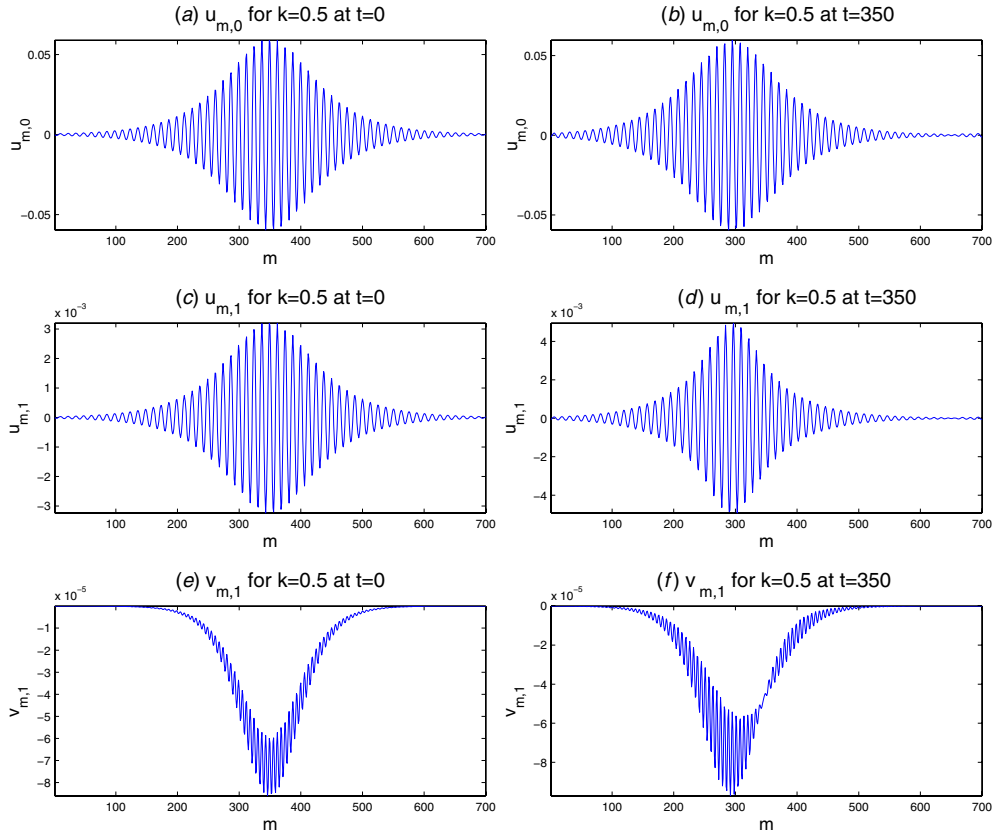

Figure 9. Plots of displacements of the three main chains ($u_{m,0}$, $u_{m,1}$ and $v_{m,1}$) against lattice site m at $t = 0$ and $t = 350$, for $k = 0.5$. See section 3.4 for more details.

3.5. Stationary breather with $\mathcal{O}(1)$ parameters

The numerical results presented in the previous sections all feature parameters with large spring constant Ω (see (2.1)), since this choice guarantees that the parameter γ, defined by (2.37), is small. We now present results of a simulation in which all the parameters are $\mathcal{O}(1)$. We choose $k = \pi$, $h = 0.5$, $\varepsilon = 0.03$, $A = 1.0$, $a = 0.0$, $b = 0.2$, $\lambda = 1.0$ and $\Omega = 0.5$ and a lattice of size $M_S = 120$, $N_S = 10$. (Note that we still require $0 < \varepsilon \ll 1$ in order for our three-chain asymptotic analysis to be valid.) In this case, the temporal frequency of the carrier wave is $\omega = 2.0616$, the period of oscillation is $T = 2\pi/\omega = 3.0478$ and solving (2.37) we find $\gamma = 0.056$—still relatively small.

The breather is initially situated at the centre of the lattice as shown in figures 10(*a*) and (*c*), and the corresponding total energy is $H = 0.157657$. Figures 10(*b*) and (*d*) show the breather after approximately 30 oscillations ($t = 29.53T = 90$). The total energy does not alter significantly over this time: $\Delta H/H = 6.3429^{-6}$. The final main-chain energy is $H_0(t = 90) = 0.1558$, which is again close to the initial value $H_0(t = 0) = 0.1567$ (the change being $\Delta H_0/H_0 = 0.0058$). Our asymptotic estimate of H_0, given by (2.47), is 0.1568. The energy in either side chain is initially 4.5446×10^{-4} at $t = 0$ (in good agreement with the $t = 0$ asymptotic estimate of $H_1 = 4.5150 \times 10^{-4}$), but at $t = 90$, $H_1 = 8.9485 \times 10^{-4}$—a

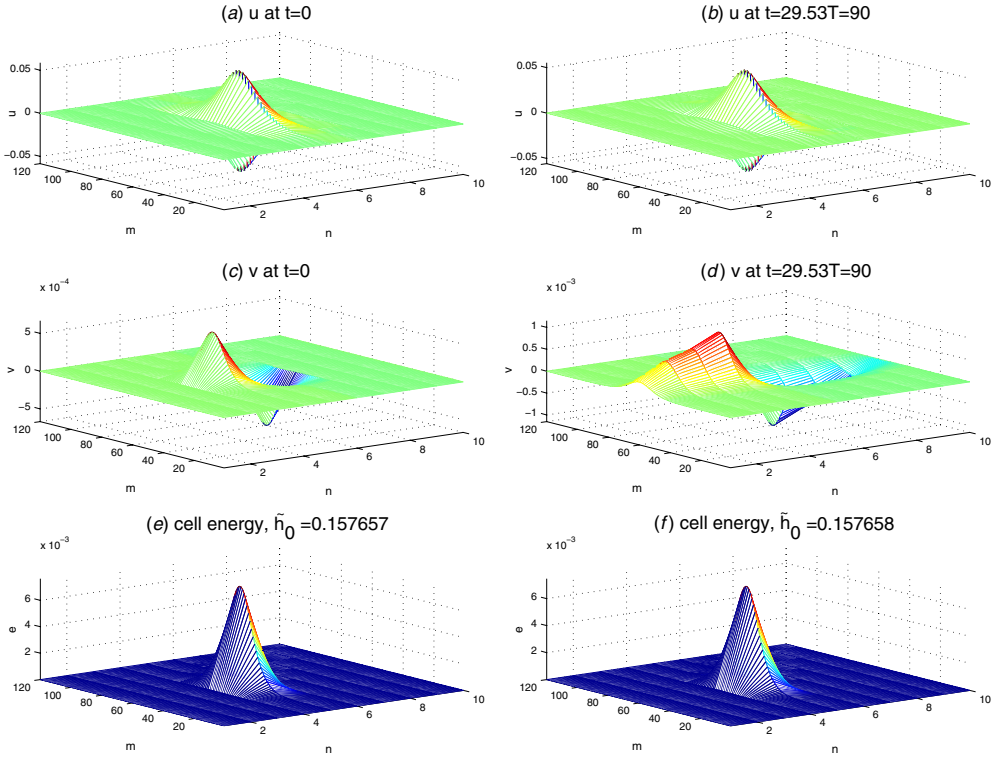

Figure 10. The displacements and energy density of a stationary breather in the square lattice, plotted as a function of lattice position (m, n), at times $t = 0$ ((a), (c), (e)) and $t = 90$ ((b), (d), (f)). (a), (b) Longitudinal displacements $u_{m,n}$; (c), (d) vertical displacements $v_{m,n}$; (e), (f) cell energy density $e_{m,n}$. See section 3.5 for more details.

significant increase. Nonetheless, figures 10(e) and (f) illustrate that the breather does not lose its localized structure even after 30 oscillations.

To investigate the shape changes further, we run the simulations to longer times and plot the breather widths in m- and n-directions, W_{mbr} and W_{nbr}, using a lattice of size $M_S = 200$ and $N_S = 10$. Figure 11 shows that both widths increase monotonically and significantly, with the n-width in particular growing by almost a factor of about 6.5 over the long-time simulation. At $t = 0$, $W_{mbr} = 9.2873$ and $W_{nbr} = 0.0780$, and after approximately 230 oscillations the corresponding values are 11.3651 and 0.5064, respectively.

The variation of the energy, $E_{\rm br}$, in a box of size 100×5 is also small in this case: the initial value of 0.16 decreases by only 0.0038 over the time interval $0 < t < 700$. Even though this variation is small, and such a breather may be termed long-lived, it is large enough to state that such a breather is not an exact solution of the lattice. Our earlier simulations of moving breathers with $\Omega \gg 1$ showed variations in $E_{\rm br}$ of $\mathcal{O}(10^{-6})$ for moving breathers and even smaller variations for stationary breathers.

3.6. Moving breather with $\mathcal{O}(1)$ parameters and $k = 0.5$

In this section, we focus on the breather with $k = 0.5$, $\varepsilon = 0.03$, $A = 1.0$, in a lattice with $\Omega = 1.0$, $h = 1.0$, $a = 0.0$, $b = -1.0$, $\lambda = -1.0$ and of size $M_S = 500$, $N_S = 10$. The

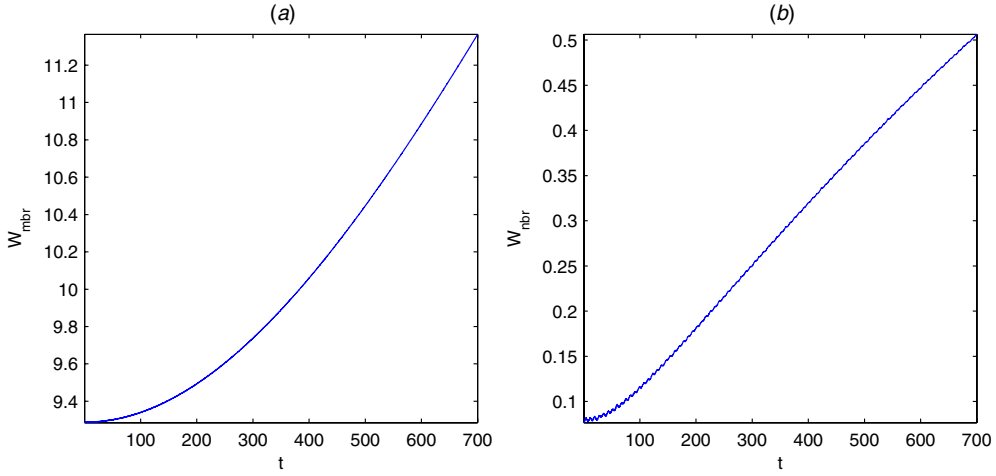

Figure 11. Plot of the breather widths W_{mbr} and W_{nbr} in m- and n-directions against time, for $k = 0.5$ and $\Omega = 0.5$. See section 3.5 for more details.

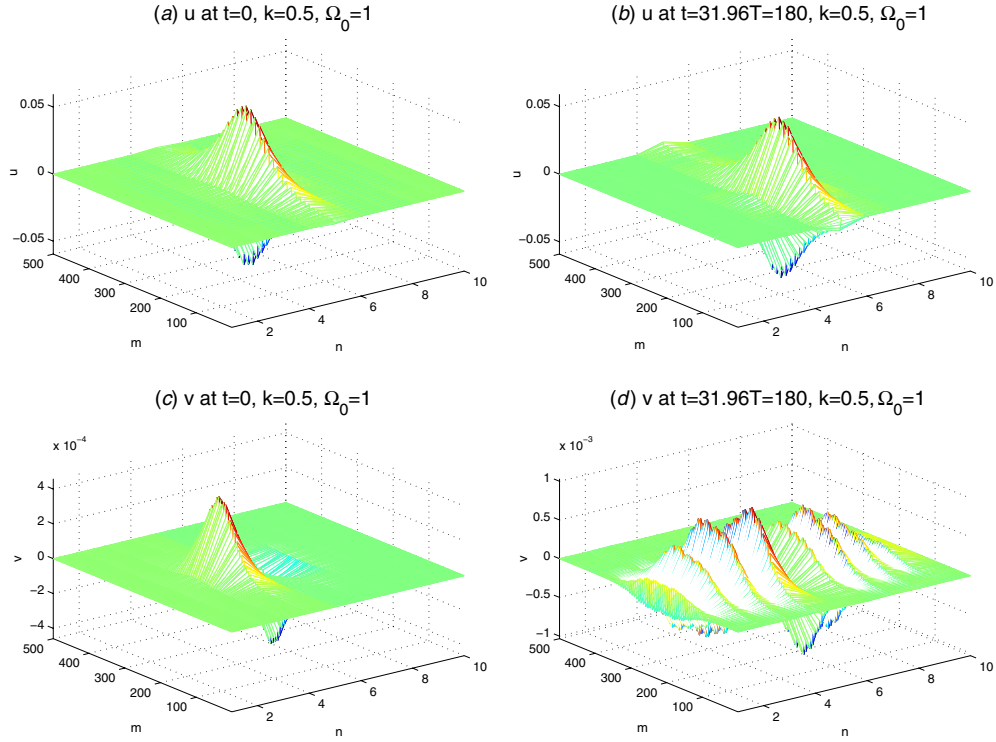

Figure 12. Displacements as a function of lattice position (m, n), for moving breather in lattice with $\Omega = 1 = \mathcal{O}(1)$ and $k = 0.5$. (a) $u_{m,n}$ at $t = 0$, (b) $u_{m,n}$ at $t = 180$, (c) $v_{m,n}$ at $t = 0$, (d) $v_{m,n}$ at $t = 180$. See section 3.6 for more details.

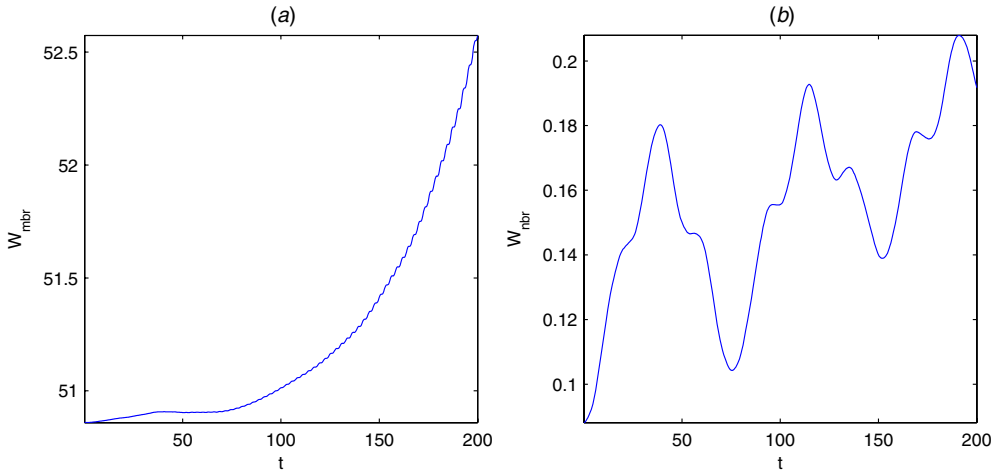

Figure 13. Breather widths as a function of time for the moving breather with $\Omega = 1$ and $k = 0.5$: (*a*) Breather width W_{mbr} in the m-direction and (*b*) breather width W_{nbr} in the n-direction. See section 3.6 for more details.

asymptotic estimate of velocity given by (2.14) is $v = -0.4297$, and the breather frequency is $\omega = 1.1157$, giving an oscillation time period of $T = 5.6315$.

Figures 12(*a*) and (*c*) show the breather at $t = 0$, while figures 12(*b*) and (*d*) show the breather at time $t = 180$, after almost 32 oscillations. Clearly, the v-component of the breather has been deformed more significantly in the n-direction than in the m-direction (or than the u-component in either direction). However, the breather retains its localized structure since the u-component of the central chain dominates ($u_{m,0} \gg v_{m,1}$). The difference between the asymptotic (2.14) and numerical velocities ($v_{\text{num}} = -0.4425$) is 2.28%.

At time $t = 0$ the main- and side-chain energies are $H_0 = 0.2522$ and $H_1 = 9.5317 \times 10^{-4}$, close to the asymptotic estimates of $H_0 = 0.2523$ and $H_1 = 9.4329 \times 10^{-4}$, respectively. At $t = 180$, $H_0 = 0.2491$ which is only slightly less than the value at $t = 0$; however, $H_1 = 0.0024$ which is larger than the value at $t = 0$ by a factor of about 2.5. Measuring the energy E_{br} in a box of length 100 and width 5 centred on the breather, we find $E_{\text{br}} = 0.18$ at $t = 0$, and this quantity decreases in value by only about 0.0015 units over the period of the simulation ($0 \leqslant t \leqslant 300$)—a loss of less than 1% over more than 53 oscillations.

Figure 13 shows the m-width of the breather W_{mbr} increasing a little over the simulation: initially it grows very slightly and then stays fixed for a time, before increasing at an accelerating rate. At $t = 0$, $W_{mbr} = 50.85$, and (approximately) 36 oscillations later, $W_{mbr} = 52.57$. n-width W_{nbr} exhibits much more unusual behaviour, generally increasing but undergoing relatively large oscillations. At $t = 0$, $W_{nbr} = 0.088$, increasing to $W_{nbr} = 0.1917$ by the time $t = 200$.

4. Conclusions

In this paper, we have applied asymptotic methods to find approximations to discrete breathers in a two-dimensional spring-mass lattice system (Fermi–Pasta–Ulam–Tsingou (FPUT) or Klein–Gordon (KG) type). In our model, the vibration has two degrees of freedom at each lattice site. It makes this model considerably more complicated than the scalar one-component lattice analysed in some previous papers (for example, [11]). We assume that the amplitude

of a breather's disturbance is largely confined to three main chains and that motion in the remaining chains is too small to affect significantly our calculations. Thus, we focus on the coupled motion of the central chain and two side chains, assuming that the motion of these three main chain in isolation is sufficient to describe such breathers. We simplify our approach by assuming that the motion in the two side chains is symmetric, and so described by only two variables, and the motion in the central chain is in one direction. Thus, we obtain a system of three coupled one-dimensional lattice equations.

Marin *et al* [21, 22] have performed numerical investigations of breather dynamics in such two-dimensional lattices. Their results suggest that moving breather modes exist and that the lattice exhibits a strong directional preference whereby breathers can only move along symmetries of the lattice and in no other direction.

We use the discrete multiple-scales method to reduce the equations of motion for the three main chains in this FPUT–KG lattice to a system of two nonlinear Schrödinger equations ((2.24) and(2.25)). Requiring this system to have similar solutions leads to the identification of an important correlation parameter γ (2.36), between the leading order functions in the solution ansatz for the central chain and side chain.

The ansatz used herein is quite distinct from that used by Butt and Wattis for the one-component, two-dimensional lattice; in [5, 6] they assumed that the stationary breather was circularly symmetric and that, following a simple rescaling, moving breathers had a similar symmetry, with amplitude being dependent on a (scaled, vector) displacement from the mode centre in the two lattice directions. There, moving breathers were elongated *perpendicular* to the direction of travel. Here we find elongated moving breathers elongated *in* the direction of travel (as well as elongated static breathers). Thus, we note significant differences in behaviour between scalar- and vector-valued lattices.

In this paper, we have built a typical nonlinear mechanical (vector-valued) lattice and shown that a breather mode exists, is stable and relevant to the long-time dynamics of the lattice. Cuevas *et al* [11] have investigated localized oscillations in both ordered and disordered two-dimensional scalar lattices (discrete breathers and Anderson modes). They have also analysed the bifurcations which lead to their creation. It would be interesting to see the results of a similar study on the more complicated vector-valued lattice equations that we have analysed here. As noted in the above paragraph, there may again be significant differences between scalar and vector lattices.

In sections 2.6 and 2.7, we investigated the region where bright soliton solutions exist for the two-dimensional mechanical (two-component, vector) FPUT–KG lattice with a polynomial potential. In our analysis we assume the correlation parameter γ to be a small real number, and we also consider $\Omega \gg 1$ to allow a theoretical approach to calculating explicit approximations to the breathers. As well as obtaining expressions for the breather energy, we are able to illustrate the regions where bright soliton solutions exist (figure 2) in the two-dimensional spring-mass system.

Numerical simulations presented in section 3 reveal interesting properties of breathers. For $\Omega \gg 1$, the asymptotic approximation to breathers is good: we observe that their evolution is almost lossless and they are localized in both directions, extremely so in one direction. Moving breathers are extremely localized perpendicular to their direction of travel. For $\Omega = \mathcal{O}(1)$, the simulations show much greater modifications to shape over time, particularly in the rate at which a breather's width increases. In addition, we see a noticeable amount of energy left behind at the initial position of the breather, which will spread out over longer timescales. This is particularly notable in the case of wavenumber $k < \pi/2$. This shows that the asymptotic approximation is not so good in the case $\Omega = \mathcal{O}(1)$ as when $\Omega \gg 1$. The results of our asymptotic calculations and simulations support and justify the term 'quodons'

for these breathers which are dominated by motion in just a few chains and by motion in one direction (the u-component). We have also compared the breather's velocity and the leading order values of the energy, H_0, from numerical calculations and asymptotic calculations. The results show a good match over a range of parameters.

We have observed that in moving breathers, particularly for $\Omega = \mathcal{O}(1)$, energy is slowly transferred from the central chain to the side chains as the wave passes though the two-dimensional spring-mass lattice system. Thus it would appear that, while the moving breather may be a relatively long-lived mode, it is not an exact solution.

Marin *et al* [22, 23] have already given some convincing numerical evidence that moving breathers exist in hexagonal and square lattices and that these breathers travel only along lattice directions. Hence, in the near future, we aim to use this triple chain approximation to study breathers in the hexagonal FPU–KG lattice.

Acknowledgments

We would like to thank the referees for their helpful comments and suggestions on the manuscript.

Appendix A. Energy definitions

We define the main-chain energy (that is, the chain $n = 0$) by

$$\begin{aligned} H_0 = \sum_m & \frac{1}{2}\dot{u}_{m,0}^2 + \frac{1}{2}\Omega^2 u_{m,0}^2 + \frac{1}{4}\lambda u_{m,0}^4 + \frac{1}{2}(u_{m+1,0} - u_{m,0})^2 \\ & + \frac{1}{2h} v_{m,1}(u_{m,1} - u_{m,0})^2 + \frac{1}{8h^2}(u_{m,1} - u_{m,0})^4 + \frac{1}{2h^2} v_{m,1}^2 (u_{m,1} - u_{m,0})^2 \\ & + \frac{1}{3}a(u_{m+1,0} - u_{m,0})^3 + \frac{1}{4}b(u_{m+1,0} - u_{m,0})^4 \end{aligned} \tag{A.1}$$

(see [7]). Again using the symmetry, we deduce that the energies of the two side chains are identical, that is, $H_{-1} = H_1$. Following [7], or using the assumption that only $u_{m,1}$, $v_{m,1}$, $u_{m,0}$ are significant, we find the expression for the side-chain energy:

$$\begin{aligned} H_1 = \sum_m & \frac{1}{2}\dot{u}_{m,1}^2 + \frac{1}{2}\dot{v}_{m,1}^2 + \frac{1}{2}\Omega^2(u_{m,1}^2 + v_{m,1}^2) + \frac{1}{4}\lambda(u_{m,1}^2 + v_{m,1}^2)^2 + \frac{1}{2}(u_{m+1,1} - u_{m,1})^2 \\ & + \frac{1}{2h}(u_{m+1,1} - u_{m,1})(v_{m+1,1} - v_{m,1})^2 + \frac{1}{8h^2}(v_{m+1,1} - v_{m,1})^4 \\ & - \frac{1}{2h^2}(u_{m+1,1} - u_{m,1})^2(v_{m+1,1} - v_{m,1})^2 + \frac{1}{2}v_{m,1}^2 - \frac{1}{4h}v_{m,1}u_{m,1}^2 \\ & + \frac{1}{4h}v_{m,1}(u_{m,1} - u_{m,0})^2 + \frac{1}{16h^2}u_{m,1}^4 + \frac{1}{16h^2}(u_{m,1} - u_{m,0})^4 \\ & - \frac{1}{4h^2}v_{m,1}^2 u_{m,1}^2 - \frac{1}{4h^2}v_{m,1}^2(u_{m,1} - u_{m,0})^2 + \frac{1}{3}a(u_{m+1,1} - u_{m,1})^3 \\ & + \frac{1}{2h}a(u_{m+1,1} - u_{m,1})^2(v_{m+1,1} - v_{m,1})^2 + \frac{1}{4h}a v_{m,1}^2 u_{m,1}^2 \\ & + \frac{1}{4h}a v_{m,1}^2(u_{m,1} - u_{m,0})^2 + \frac{1}{3}a v_{m,1}^3 + \frac{1}{4}b(u_{m+1,1} - u_{m,1})^4 + \frac{1}{4}b v_{m,1}^4. \end{aligned} \tag{A.2}$$

In order to determine the position of the breather, we define the 'cell energy' $e_{m,n}$ by

$$e_{m,n} = \frac{1}{2}\dot{u}_{m,n}^2 + \frac{1}{2}\dot{v}_{m,n}^2 + \frac{\Omega^2}{2}(u_{m,n}^2 + v_{m,n}^2) + \frac{\lambda}{4}(u_{m,n}^2 + v_{m,n}^2)^2 + \frac{1}{4}(u_{m+1,n} - u_{m,n})^2$$

$$
\begin{aligned}
&+\frac{1}{4}(u_{m,n}-u_{m-1,n})^2+\frac{1}{2h}(u_{m+1,n}-u_{m,n})(v_{m+1,n}-v_{m,n})^2\\
&+\frac{1}{8h^2}(v_{m+1,n}-v_{m,n})^4-\frac{1}{2h^2}(u_{m+1,n}-u_{m,n})^2(v_{m+1,n}-v_{m,n})^2\\
&+\frac{1}{2}(v_{m,n+1}-v_{m,n})^2+\frac{1}{2h}(v_{m,n+1}-v_{m,n})(u_{m,n+1}-u_{m,n})^2\\
&+\frac{1}{8h^2}(u_{m,n+1}-u_{m,n})^4-\frac{1}{2h^2}(v_{m,n+1}-v_{m,n})^2(u_{m,n+1}-u_{m,n})^2\\
&+a\left(\frac{1}{3}(u_{m+1,n}-u_{m,n})^3+\frac{1}{2h}(u_{m+1,n}-u_{m,n})^2(v_{m+1,n}-v_{m,n})^2\right)\\
&+a\left(\frac{1}{3}(v_{m,n+1}-v_{m,1})^3+\frac{1}{2h}(v_{m,n+1}-v_{m,1})^2(u_{m,n+1}-u_{m,n})^2\right)\\
&+\frac{1}{4}b(u_{m+1,n}-u_{m,n})^4+\frac{1}{4}b(v_{m,n+1}-v_{m,n})^4. \qquad \text{(A.3)}
\end{aligned}
$$

Hence the total energy of the system is given by $H=\sum_m\sum_n e_{m,n}$, and in the three-chain approximation we have $H=H_0+2H_1$.

References

[1] Archilla J F R, Cuevas J, Alba M D, Naranjo M and Trillo J M 2006 Discrete breathers for understanding reconstructive mineral processes at low temperatures *J. Phys. Chem.* B **110** 24112–20

[2] Aubry S and Cretegny T 1998 Mobility and reactivity of discrete breathers *Physica* D **119** 34–46

[3] Bambusi D 1996 Exponential stability of breathers in Hamiltonian networks of weakly coupled oscillators *Nonlinearity* **9** 433–57

[4] Barbi M, Cocco S and Peyrard M 1999 Helicoidal model for DNA opening *Phys. Lett.* A **253** 358–69

[5] Butt I A and Wattis J A D 2006 Discrete breathers in a two dimensional hexagonal Fermi–Pasta–Ulam lattice *J. Phys. A: Math. Gen.* **40** 1239–64

[6] Butt I A and Wattis J A D 2006 Discrete breathers in a two-dimensional Fermi–Pasta–Ulam lattice *J. Phys. A: Math. Gen.* **39** 4955–84

[7] Butt I A 2006 Discrete breathers in one- and two-dimensional lattices *PhD Thesis* University of Nottingham http://etheses.nottingham.ac.uk/archive/00000238

[8] Campbell D K 2004 Fresh breather *Nature* **432** 455–6

[9] Campbell D K, Flach S and Kivshar Y S 2004 Localizing energy through non-linearity and discreteness *Phys. Today* **57** 43–9

[10] Christiansen P L, Lomdahl P S and Muto V 1990 On a Toda lattice model with a transversal degree of freedom *Nonlinearity* **4** 477–501

[11] Cuevas J, Archilla J F R, Palmero F and Romero F R 2001 Numerical study of two-dimensional disordered Klein–Gordon lattices with cubic soft anharmonicity *J. Phys. A: Math. Gen.* **34** L221–30

[12] Fermi E, Pasta J and Ulam S 1974 Studies of nonlinear problems: I *Los Alamos Scientific Report LA-1940* (originally unpublished in 1955) Later published in *Lectures Appl. Math* **15** 143–65

[13] Flach S, Klado K and MacKay R S 1997 Energy thresholds for discrete breather in one-, two- and three-dimensional lattices *Phys. Rev. Lett.* **78** 1207–10

[14] Flach S, Kladko K and Willis C R 1994 Localized existences in two-dimensional Hamiltonian lattices *Phys. Rev.* E **50** 2293–303

[15] Flach S and Willis C R 1993 Localized excitations in a discrete Klein–Gordon system *Phys. Lett.* A **181** 232–8

[16] Flach S and Willis C R 1994 Movability of localized excitations in nonlinear discrete systems: a separatrix problem *Phys. Rev. Lett.* **72** 1777–81

[17] Flach S and Willis C R 1998 Discrete breathers *Phys. Rep.* **259** 181–243

[18] Homma S and Takeno S 1984 A coupled base-rotator model for structure and dynamics of DNA *Prog. Theor. Phys.* **72** 679–93

[19] Kevrekidis P G, Rasmussen K Ø and Bishop A R 2000 Two-dimensional discrete breathers: construction, stability, and bifurcations *Phys. Rev.* E **61** 2006–9

[20] MacKay R S and Aubry S 1994 Proof of existence of breathers for time reversible or Hamiltonian networks of weakly coupled oscillators *Nonlinearity* **7** 1623–43

[21] Marin J L, Eilbeck J C and Russell F M 2000 2-D breathers and applications *Nonlinear Science at the Dawn of the 21st Century* (*Lecture Notes in Physics* vol 542) ed P L Christiansen, M P Sorensen and A C Scott (Berlin: Springer) pp 293–305
[22] Marin J L, Eilbeck J C and Russell F M 1998 Localized moving breathers in a 2D hexagonal lattice *Phys. Lett.* A **248** 225–9
[23] Marin J L, Russell F M and Eilbeck J C 2001 Breathers in cuprate-like lattices *Phys. Lett.* A **281** 21–5
[24] Muto V, Lomdahl P S and Christiansen P L 1990 Two-dimensional discrete model for DNA dynamics: longitudinal wave propagation and denaturation *Phys. Rev.* A **42** 7452–8
[25] Remoissenet M 1985 Low-amplitude breather and envelope solitons in quasi-one-dimensional physical models *Phys. Rev.* B **33** 2386–92
[26] Scott A C 1999 *Nonlinear Science* 2nd edn (Oxford: Oxford University Press)
[27] Takeno S 1990 Localized models in the long time behavior of anharmonic lattice *J. Phys. Soc. Japan* **359** 1517–20
[28] Takeno S 1990 A propagating self-localized in a one-dimensional lattices with quartic anharmonicity *J. Phys. Soc. Japan* **59** 3037–40
[29] Takeno S 1992 Theory of stationary anharmonic localized modes in solids *J. Phys. Soc. Japan* **61** 2821–34
[30] Takeno S and Hori K 1991 Self-localized modes in a pure one-dimensional lattice with cubic and quartic lattice anharmonicity *J. Phys. Soc. Japan* **60** 947–59
[31] Takeno S, Kisoda K and Sievers A J 1988 Intrinsic localized vibrational modes in anharmonic crystals *Prog. Theor. Phys. Suppl. Japan* **94** 242–69
[32] Xiao J X, Lin J T and Zhang G X 1987 The influence of longitudinal vibration on soliton excitation in DNA double helices *J. Phys. A: Math. Gen.* **20** 2425–32
[33] Zhang C T 1987 Soliton excitations in deoxyribonucleic acid (DNA) double helices *Phys. Rev.* A **35** 886–91
[34] Zhang C T 1989 Harmonic and subharmonic resonances of microwave absorption in DNA *Phys. Rev.* A **40** 2148–53